cells, which plays an important role in the atherogenic process [26].

The association between concentrations of inflammatory markers and PAOD observed in this study was consistent with previous findings that plasma sICAM-1 [9,27] and sVCAM-1 [10,27] were increased in PAOD subjects, but vWF was not [28]. Several reports have shown that adiponectin inhibits the expression of ICAM-1 and VCAM-1 [16,29], and interferes with monocyte adherence to endothelial cells and their subsequent migration to the subendothelial space, one of the initial events in the development of atherosclerosis. Thus, measuring adiponectin concentration might help to determine the progressive status of atherosclerosis.

We performed *Study* 2 to clarify the change of adiponectin between femoral artery and vein. In subjects without PAOD, the plasma concentration of adiponectin in the saphenous vein was significantly higher than that in the femoral artery. Therefore, a significant step-up of adiponectin from the femoral artery to the saphenous vein was observed in these subjects. The exact reason for the step-up of this concentration is unclear, but the production of this peptide by adipose tissue of the lower extremities may be involved. In contrast, there was no significant step-up of this peptide in PAOD subjects. Although it has not been clarified why plasma adiponectin concentration is decreased in cardiovascular disease, our results lead to the hypothesis that hypoadiponectinemia may be associated with atherosclerotic lesion itself. Previous reports of immunohistochemical studies had indicated that adiponectin adheres to injured arteries [26,30]. Another possible reason is the different amount of peripheral adiposity between with and without PAOD subjects. Furthermore, decreased peripheral adiponectin clearance from the lower extremities in PAOD subjects could not be ruled out as possible mechanism. Thus, we carried out *Study* 3. An elevated concentration of Hs-CRP, a reliable marker of inflammation, suggested that acute vascular inflammation occurred after PTA. Adiponectin may decrease as the result of the acute inflammation. A previous report had shown that adiponectin decreased immediately after the onset of acute myocardial infarction [31]. The precise mechanism of the decreased adiponectin concentrations after PTA remains unclear because only a small number of subjects were included in *Study* 3, and the adiponectin levels after PTA were not followed until Hs-CRP returned to the pre-PTA level. Furthermore, to clearly evaluate the local production of adiponectin in PAOD, examining adiponectin concentration in femoral artery and vein even after PTA is needed. It remains unclear whether the complex of endothelial dysfunction, inflammation, or decreased peripheral clearance is involved in the mechanism of decreased adiponectin levels in PAOD, and further investigation is required to verify these hypotheses.

The major limitation was that several important determinants of plasma adiponectin level, such as body fat content and waist circumference, were not measured in our study. Instead of these measurements, we included HOMA and BMI in the analysis of this study. Previous reports had shown that body fat content, especially central adiposity, is one of the determinants of adiponectin level [32]. On the other hand, the different localization of fat mass itself influences cardiovascular risk factors, such as total cholesterol, triglycerides, and HDL-cholesterol [33]. In our study (both *Study* 1 and *Study* 2), the clinical characteristics between subjects with and without PAOD were not significantly different, except for HDL-cholesterol in *Study* 1 and prevalence of ischemic heart disease in *Study* 2.

In conclusion, the present findings demonstrated that the plasma adiponectin concentration is decreased in subjects with PAOD in proportion to the severity of the disease. Adiponectin concentration could be a marker of the existence of atherosclerosis, especially with an inflammatory signature. These findings suggest an important role of adiponectin in atherosclerosis and may serve as the basis for further evaluation of circulating adiponectin as a potential biochemical marker for atherosclerosis.

Acknowledgements

This study was supported by the Program for Promotion of Fundamental Studies in Health Sciences of the Pharmaceuticals and Medical Devices Agency (PMDA). We are indebted to Mrs. Sachiyo Tanaka and Mrs. Yoko Saito for their excellent technical assistance.

References

[1] Rossi E, Biasucci LM, Citterio F, et al. Risk of myocardial infarction and angina in patients with severe peripheral vascular disease: predictive role of C-reactive protein. Circulation 2002;105:800–3.
[2] Libby P, Ridker PM, Maseri A. Inflammation and atherosclerosis. Circulation 2002;105:1135–43.
[3] Ridker PM, Cushman M, Stampfer MJ, Tracy RP, Hennekens CH. Plasma concentration of C-reactive protein and risk of developing peripheral vascular disease. Circulation 1998;97:425–8.
[4] Ross R. The pathogenesis of atherosclerosis: a perspective for the 1990s. Nature 1993;362:801–9.
[5] Dustin ML, Rothlein R, Bhan AK, Dinarello CA, Springer TA. Induction by IL 1 and interferon-gamma: tissue distribution, biochemistry, and function of a natural adherence molecule (ICAM-1). J Immunol 1986;137:245–54.
[6] Pober JS, Gimbrone Jr MA, Lapierre LA, et al. Overlapping patterns of activation of human endothelial cells by interleukin 1, tumor necrosis factor, and immune interferon. J Immunol 1986;137:1893–6.
[7] Davies MJ, Gordon JL, Gearing AJ, et al. The expression of the adhesion molecules ICAM-1, VCAM-1, PECAM, and E-selectin in human atherosclerosis. J Pathol 1993;171:223–9.
[8] Peter K, Nawroth P, Conradt C, et al. Circulating vascular cell adhesion molecule-1 correlates with the extent of human atherosclerosis in contrast to circulating intercellular adhesion molecule-1, E-selectin, P-selectin, and thrombomodulin. Arterioscler Thromb Vasc Biol 1997;17:505–12.
[9] Pradhan AD, Rifai N, Ridker PM. Soluble intercellular adhesion molecule-1, soluble vascular adhesion molecule-1, and the development of symptomatic peripheral arterial disease in men. Circulation 2002;106:820–5.

[10] De Caterina R, Basta G, Lazzerini G, et al. Soluble vascular cell adhesion molecule-1 as a biohumoral correlate of atherosclerosis. Arterioscler Thromb Vasc Biol 1997;17:2646–54.
[11] Cines DB, Pollak ES, Buck CA, et al. Endothelial cells in physiology and in the pathophysiology of vascular disorders. Blood 1998;91:3527–61.
[12] Blann AD, McCollum CN, Lip GY. Relationship between plasma markers of endothelial cell integrity and the Framingham cardiovascular disease risk-factor scores in apparently healthy individuals. Blood Coagul Fibrinolysis 2002;13:513–8.
[13] Arita Y, Kihara S, Ouchi N, et al. Paradoxical decrease of an adipose-specific protein, adiponectin, in obesity. Biochem Biophys Res Commun 1999;257:79–83.
[14] Hotta K, Funahashi T, Arita Y, et al. Plasma concentrations of a novel, adipose-specific protein, adiponectin, in type 2 diabetic patients. Arterioscler Thromb Vasc Biol 2000;20:1595–9.
[15] Iwashima Y, Katsuya T, Ishikawa K, et al. Hypoadiponectinemia is an independent risk factor for hypertension. Hypertension 2004;43:1318–23.
[16] Ouchi N, Kihara S, Arita Y, et al. Novel modulator for endothelial adhesion molecules: adipocyte-derived plasma protein adiponectin. Circulation 1999;100:2473–6.
[17] Kumada M, Kihara S, Sumitsuji S, et al. Association of hypoadiponectinemia with coronary artery disease in men. Arterioscler Thromb Vasc Biol 2003;23:85–9.
[18] McDermott MM, Greenland P, Liu K, et al. Leg symptoms in peripheral arterial disease: associated clinical characteristics and functional impairment. JAMA 2001;286:1599–606.
[19] Report of the expert committee on the diagnosis and classification of diabetes mellitus. Diabetes Care 2003;26(Suppl. 1):S5–20.
[20] McDermott MM, Criqui MH, Liu K, et al. Lower ankle/brachial index, as calculated by averaging the dorsalis pedis and posterior tibial arterial pressures, and association with leg functioning in peripheral arterial disease. J Vasc Surg 2000;32:1164–71.
[21] Iwashima Y, Katsuya T, Ishikawa K, et al. Association of hypoadiponectinemia with smoking habit in men. Hypertension 2005;45:1094–100.
[22] Ouchi N, Kihara S, Funahashi T, et al. Reciprocal association of C-reactive protein with adiponectin in blood stream and adipose tissue. Circulation 2003;107:671–4.
[23] Fiotti N, Giansante C, Ponte E, et al. Atherosclerosis and inflammation. Patterns of cytokine regulation in patients with peripheral arterial disease. Atherosclerosis 1999;145:51–60.
[24] Ouchi N, Ohishi M, Kihara S, et al. Association of hypoadiponectinemia with impaired vasoreactivity. Hypertension 2003;42:231–4.
[25] Yamauchi T, Kamon J, Waki H, et al. The fat-derived hormone adiponectin reverses insulin resistance associated with both lipoatrophy and obesity. Nat Med 2001;7:941–6.
[26] Ouchi N, Kihara S, Arita Y, et al. Adipocyte-derived plasma protein, adiponectin, suppresses lipid accumulation and class A scavenger receptor expression in human monocyte-derived macrophages. Circulation 2001;103:1057–63.
[27] Blann AD, Seigneur M, Steiner M, Miller JP, McCollum CN. Circulating ICAM-1 and VCAM-1 in peripheral artery disease and hypercholesterolaemia: relationship to the location of atherosclerotic disease, smoking, and in the prediction of adverse events. Thromb Haemost 1998;79:1080–5.
[28] Philipp CS, Cisar LA, Kim HC, et al. Association of hemostatic factors with peripheral vascular disease. Am Heart J 1997;134:978–84.
[29] Kawanami D, Maemura K, Takeda N, et al. Direct reciprocal effects of resistin and adiponectin on vascular endothelial cells: a new insight into adipocytokine-endothelial cell interactions. Biochem Biophys Res Commun 2004;314:415–9.
[30] Okamoto Y, Arita Y, Nishida M, et al. An adipocyte-derived plasma protein, adiponectin, adheres to injured vascular walls. Horm Metab Res 2000;32:47–50.
[31] Kojima S, Funahashi T, Sakamoto T, et al. The variation of plasma concentrations of a novel, adipocyte derived protein, adiponectin, in patients with acute myocardial infarction. Heart 2003;89:667.
[32] Cnop M, Havel PJ, Utzschneider KM, et al. Relationship of adiponectin to body fat distribution, insulin sensitivity and plasma lipoproteins: evidence for independent roles of age and sex. Diabetologia 2003;46:459–69.
[33] Tanko LB, Bagger YZ, Alexandersen P, Larsen PJ, Christiansen C. Peripheral adiposity exhibits an independent dominant antiatherogenic effect in elderly women. Circulation 2003;107:1626–31.

Original Article

Pioglitazone but Not Glibenclamide Improves Cardiac Expression of Heat Shock Protein 72 and Tolerance Against Ischemia/Reperfusion Injury in the Heredity Insulin-Resistant Rat

Yayoi Taniguchi,[1] Tatsuhiko Ooie,[1] Naohiko Takahashi,[2] Tetsuji Shinohara,[2] Mikiko Nakagawa,[1] Hidetoshi Yonemochi,[1] Masahide Hara,[2] Hironobu Yoshimatsu,[2] and Tetsunori Saikawa[1]

We tested the hypothesis that pioglitazone could restore expression of heat shock protein (HSP)72 in insulin-resistant rat heart. At 12 weeks of age, male Otsuka Long-Evans Tokushima Fatty (OLETF) rats and control (LETO) rats were treated with pioglitazone (10 mg · kg^{-1} · day^{-1}) or glibenclamide (5 mg · kg^{-1} · day^{-1}) for 4 weeks. Thereafter, hyperthermia (43°C for 20 min) was applied. In response to hyperthermia, the activation of serine/threonine kinase Akt depending on phosphatidylinositol 3 (PI3) kinase was necessary for cardiac expression of HSP72. Hyperthermia-induced activation of Akt and HSP72 expression were depressed in OLETF rat hearts. Pioglitazone but not glibenclamide improved insulin sensitivity in OLETF rats, which was associated with the restoration of Akt activation and HSP72 expression. In experiments with isolated perfused heart, reperfusion-induced cardiac functional recovery was suppressed in OLETF rat hearts, which was improved by pioglitazone but not glibenclamide. Our results suggest that PI3 kinase–dependent Akt activation, an essential signal for HSP72 expression, is depressed in the heart in insulin-resistant OLETF rats, and the results suggest also that the restoration of HSP72 expression and tolerance against ischemia/reperfusion injury by treatment with pioglitazone might be due to an improvement of insulin resistance, leading to restoration of impaired PI3 kinase–dependent Akt activation in response to hyperthermia. *Diabetes* 55:2371–2378, 2006

Heat shock protein (HSP)72, a member of the HSP family, has been reported to be involved predominantly in cardioprotection (1–4). We have shown that induction of HSP72 by either hyperthermia or oral administration of geranylgeranylacetone (GGA) leads to protection against ischemia/reperfusion injury (5–8). However, information is very limited with respect to the impact of insulin resistance and type 2 diabetes on the expression of HSP72. Kurucz et al. (9) reported that the expression of HSP72 mRNA in skeletal muscle of patients with type 2 diabetes is decreased, which correlates with the parameters of insulin resistance. Consistent with this, we have shown attenuated cardiac HSP72 expression in response to GGA in insulin-resistant rats produced by a high-fat diet (10). Skeletal muscle, liver, and heart are known to be targeted organs of insulin resistance (11–13). However, the mechanisms underlying the depressed expression of HSP72 in insulin-resistant organs are unclear. Recently, thiazolidinediones, including pioglitazone, have been demonstrated to improve insulin resistance experimentally and clinically (14,15). Whereas sulfonylurea including glibenclamide stimulates endogenous insulin secretion through blockade of ATP-sensitive potassium channels on pancreatic β-cells, pioglitazone, a synthetic peroxisome proliferator–activated receptor-γ (PPAR-γ) agonist, does not stimulate insulin release from pancreatic β-cells (14,15). It is therefore interesting to compare the effects of treatment with pioglitazone and treatment with glibenclamide on the expression of HSP72 in the insulin-resistant animal model.

Activation of the serine/threonine kinase Akt promotes survival of some cell types including cardiomyocytes (16). Hyperthermia is known to cause Akt activation, and experimental evidence indicates that hyperthermia-induced activation of Akt can involve either a phosphatidylinositol 3 (PI3) kinase–dependent or a PI3 kinase–independent pathway (17,18). However, little is known about the involvement of Akt in hyperthermia-induced HSP72 expression in the heart. We have demonstrated recently that PI3 kinase–dependent Akt activation is essential for expression of HSP72 (19). In the present study, therefore, we tested the hypothesis that *1*) depressed cardiac HSP72 expression in insulin-resistant rats is related to depressed PI3 kinase–dependent Akt activation in response to hyperthermia and that *2*) treatment with pioglitazone improves this depressed response, resulting in restoration of cardiac expression of HSP72, which is associated with the protection against ischemia/reperfusion injury.

RESEARCH DESIGN AND METHODS

All experimental procedures were carried out in accordance with the guidelines of the Physiological Society of Oita University, Japan, for the care and use of laboratory animals.

From the [1]Department of Cardiovascular Science, Faculty of Medicine, Oita University, Oita, Japan; and the [2]Department of Internal Medicine 1, Faculty of Medicine, Oita University, Oita, Japan.

Address correspondence and reprint requests to Naohiko Takahashi, MD, PhD, Department of Internal Medicine 1, Faculty of Medicine, Oita University, 1-1 Idaigaoka, Yufu, Oita 879-5593, Japan. E-mail: takanao@med.oita-u.ac.jp.

CPP, coronary perfusion pressure; GGA, geranylgeranylacetone; HSP, heat shock protein; LVDP, left ventricular developed pressure; OGTT, oral glucose tolerance test; PI3, phosphatidylinositol 3; PPAR-γ, peroxisome proliferator–activated receptor-γ; STZ, streptozotocin.

Received for publication 25 February 2006 and accepted in revised form 22 May 2006.

DOI: 10.2337/db06-0268

TABLE 1
Basic characteristics of experimental groups after 4-week treatment with vehicle (VEH), pioglitazone (PIO), or glibenclamide (GLIB)

	LETO-VEH	LETO-PIO	LETO-GLIB	OLETF-VEH	OLETF-PIO	OLETF-GLIB	*P* value
n	14	12	12	14	12	12	
Body weight (g)	339.8 ± 4.6	346.4 ± 6.0	357.6 ± 6.9	383.4 ± 5.3*	377.6 ± 7.7*	423.5 ± 4.7*§	<0.001
LV weight (g)	0.91 ± 0.02	0.88 ± 0.03	0.96 ± 0.05	1.03 ± 0.02*	1.16 ± 0.31*	1.15 ± 0.03*§	<0.001
LV/body weight (mg/g)	2.58 ± 0.06	2.52 ± 0.09	2.73 ± 0.19	2.59 ± 0.05	2.81 ± 0.15	2.73 ± 0.06	NS
Plasma glucose (mmol/l)	5.02 ± 0.16	5.08 ± 0.29	5.08 ± 0.29	5.14 ± 0.38	4.44 ± 0.21	4.93 ± 0.25	NS
Plasma insulin (ng/ml)	1.94 ± 0.53	1.72 ± 0.50	3.32 ± 0.60	5.24 ± 1.19*	2.69 ± 0.51‡	4.79 ± 0.87	<0.01
Total cholesterol (mg/dl)	75.2 ± 1.6	73.9 ± 4.5	71.8 ± 3.0	73.5 ± 3.0	72.1 ± 5.1	72.0 ± 6.2	NS
Triglycerides (mg/dl)	32.9 ± 3.8	30.2 ± 2.2	36.0 ± 4.5	61.1 ± 6.2*	54.2 ± 2.5*	62.9 ± 6.1*	<0.001
Free fatty acid (mg/dl)	397.4 ± 21.9	348.2 ± 34.0	381.1 ± 31.0	639.5 ± 73.9†	606.4 ± 61.2*	724.0 ± 53.0*	<0.001

Data are means ± SE. *$P < 0.01$, †$P < 0.05$ vs. corresponding LETO groups; ‡$P < 0.05$, §$P < 0.01$ vs. corresponding vehicle-treated groups. LV, left ventricle.

Antibody to HSP72 (mouse) was purchased from Stressgen Biotechnologies. Antibodies to Akt, phospho-Ser^{473}-Akt, and phospho-Thr^{311}-Akt were purchased from Cell Signaling Technology. Horseradish peroxidase–tagged secondary antibodies and enhanced chemiluminescence reagents were purchased from Amersham Pharmacia Biotech. Bradford protein assay kits were purchased from Bio-Rad. Wortmannin and other chemical agents were purchased from Sigma Chemical.

Four-week-old male Otsuka Long-Evans Tokushima Fatty (OLETF) rats (70–80 g initial weight) were provided by the animal center of Tokushima Research Institute (Otsuka Pharmaceuticals). Age-matched Long-Evans Tokushima Otsuka (LETO) rats, which were developed from the same colony but do not develop insulin resistance, were used as normal controls. All rats were housed in a room illuminated daily from 700 to 1900 (12:12-h light/dark cycle) with temperature maintained at 21 ± 1°C. They were allowed free access to tap water and standard pellet rat diet. At 12 weeks of age, OLETF ($n = 90$) and LETO ($n = 90$) rats were introduced to be treated with pioglitazone (10 mg · kg^{-1} · day^{-1}, OLETF-PIO or LETO-PIO group, $n = 30$ for each), glibenclamide (5 mg · kg^{-1} · day^{-1}, OLETF-GLIB or LETO-GLIB group, $n = 30$ for each), or vehicle (OLETF-VEH or LETO-VEH group, $n = 30$ for each) orally for 4 weeks. At 16 weeks of age, each rat was anesthetized with pentobarbital (20 mg/kg i.p.) and immersed in a water bath at 43°C (hyperthermia) or 37°C (normothermia, NT) for 20 min. Rectal temperature was monitored throughout the thermo treatment to confirm changes in body temperature. In addition, some rats of the hyperthermia group ($n = 4$ for each group) were injected with either wortmannin (16 μg/kg i.v.) or saline ($n = 4$ for each group) into a tail vein 15 min before hyperthermia. Twenty-four hours after thermo treatment with normothermia or hyperthermia, following anesthesia with pentobarbital (20 mg/kg i.p.), rat hearts were isolated and prepared for Western blot analysis ($n = 4$ for each group) or isolated perfused heart experiments ($n = 7$ for each group).

Oral glucose tolerance test. At 16 weeks of age, an oral glucose tolerance test (OGTT) was performed after an overnight fast ($n = 8$ for each group). Glucose solution (2 g/kg) was administered orally, and at 0, 30, 60, 90, and 120 min, blood was drawn from a tail vein. The plasma glucose concentration was measured with a commercial test kit (GR-102; Terumo). The plasma insulin concentration was quantified using an enzyme-linked immunosorbent assay insulin kit (Morinaga Seikagaku).

Western blot analysis. Western blot analysis was performed as described (5,7,19). Briefly, rats were heparinized (500 IU/kg i.p.) and anesthetized with pentobarbital (50 mg/kg i.p.). Each heart was removed rapidly and frozen in liquid nitrogen. The frozen tissues were homogenized with lysis buffer (50 mmol/l Tris-HCl [pH 7.4], 10% glycerol, 2 mmol/l EDTA, 150 mmol/l NaCl, 1 mmol/l $MgCl_2$, 50 mmol/l glycerophosphate, 2 mmol/l Na_3VO_4, 20 mmol/l NaF, 1 mmol/l phenylmethylsulfonylfluoride, 10 μg/ml leupeptin, 10 μg/ml aprotinin, and 1% Nonidet P-40). Samples were centrifuged and the concentration of protein was measured by the Bradford method (20). An equal amount of total protein in each fraction was subjected to SDS-PAGE and transferred electrophoretically onto a polyvinylidine fluoride membrane. After blocking with 0.5% nonfat milk, the membranes were incubated with antibodies. After repeated washing, the membranes were incubated with secondary antibodies. The proteins were detected by enhanced chemiluminescence following exposure to Hyperfilm. The amount of protein on the immunoblots was quantified using National Institutes of Health image analysis software.

Isolated perfused heart experiments. Isolated perfused experiments using a Langendorff apparatus were performed as described (5,7,19). At 24 h after hyperthermia ($n = 7$ for each group) or normothermia ($n = 7$ for each group), the heart was isolated and perfused retrogradely with Krebs-Henseleit buffer (pH 7.4; 118 mmol/l NaCl, 4.7 mmol/l KCl, 2.5 mmol/l $CaCl_2$, 1.2 mmol/l $MgSO_4$, 1.2 mmol/l KH_2PO_4, 25.0 mmol/l Na_2HCO_3, 11.0 mmol/l glucose, 100 μU/ml insulin, and 3% BSA) equilibrated with 95% O_2/5% CO_2 gas mixture at 36.5°C at a constant pressure of 75 mmHg. A water-filled latex balloon was inserted through the mitral valve orifice into the left ventricle, and the left ventricular end-diastolic pressure was adjusted to 0 mmHg. During the initial 10 min of constant pressure perfusion, the perfusion flow rate was determined for each heart, which was then perfused at a determined perfusion rate using a microtube pump, while the heart was covered with water-jacketed glassware and the relative humidity was maintained at 90% or more. No-flow global ischemia was introduced for 20 min, followed by reperfusion for 30 min. The coronary effluent during the 30-min reperfusion period was collected for measurement of creatine kinase content. Creatine kinase activity was determined with a spectrophotometer by measuring NADPH production as the change in absorbance at 340 nm in the solution containing 2 mmol/l ADP, 20 mmol/l glucose, and 2 mmol/l NADP, along with 2 IU/ml of both hexokinase and glucose-6-phosphate dehydrogenase at a pH of 7.1. The reaction was initiated by addition of creatine phosphate (21). The ratio of released creatine kinase to left ventricular weight was calculated. Left ventricular pressure was monitored using a pressure transducer to obtain the peak positive and negative first derivatives of left ventricular pressure (dP/dt_{max} and dP/dt_{min}). Left ventricular developed pressure (LVDP) was defined as the difference between the left ventricular systolic and diastolic pressure. Left ventricular pressure, coronary perfusion pressure (CPP), and electrocardiogram were recorded continuously on a polygraph recorder (WS-681G; Nihon Kohden) and stored on a PCM data recorder (RD-111T; TEAC) for later analysis.

Statistical analysis. Data are expressed as means ± SE. Serial changes in plasma concentrations of glucose and insulin during OGTT and LVDP, left ventricular end-diastolic pressure, dP/dt, CPP, and heart rate during the reperfusion period were analyzed by two-way ANOVA followed by the Bonferroni-Dunn test. Comparison of physiological and serum parameters, the relative intensity of each protein, and the ratio of released creatine kinase to left ventricular weight was analyzed using one-way ANOVA, followed by the Bonferroni-Dunn test. A *P* value <0.05 was considered statistically significant.

RESULTS

Physical and metabolic characteristics. Table 1 summarizes the physical and metabolic parameters after overnight fasting in the LETO and OLETF rats after 4 weeks of treatment with vehicle, pioglitazone, or glibenclamide. When compared with the LETO-VEH group, body weight and left ventricular weight were greater in the OLETF-VEH group ($P < 0.01$ for each). Although the plasma glucose concentrations were not significantly different, the plasma insulin concentrations were higher in the OLETF-VEH group than in the LETO-VEH group ($P < 0.01$). With regard to the indexes of lipid metabolism, although the total cholesterol concentration was not significantly different, concentrations of plasma triglycerides and free fatty acid were higher in the OLETF-VEH group than in the LETO-VEH group ($P < 0.01$ and $P < 0.05$, respectively). Four weeks of treatment with pioglitazone or glibenclamide did not influence any physical and metabolic parameter in the LETO rats. In the OLETF rats, when compared with the OLETF-VEH group, the OLETF-PIO group had lower

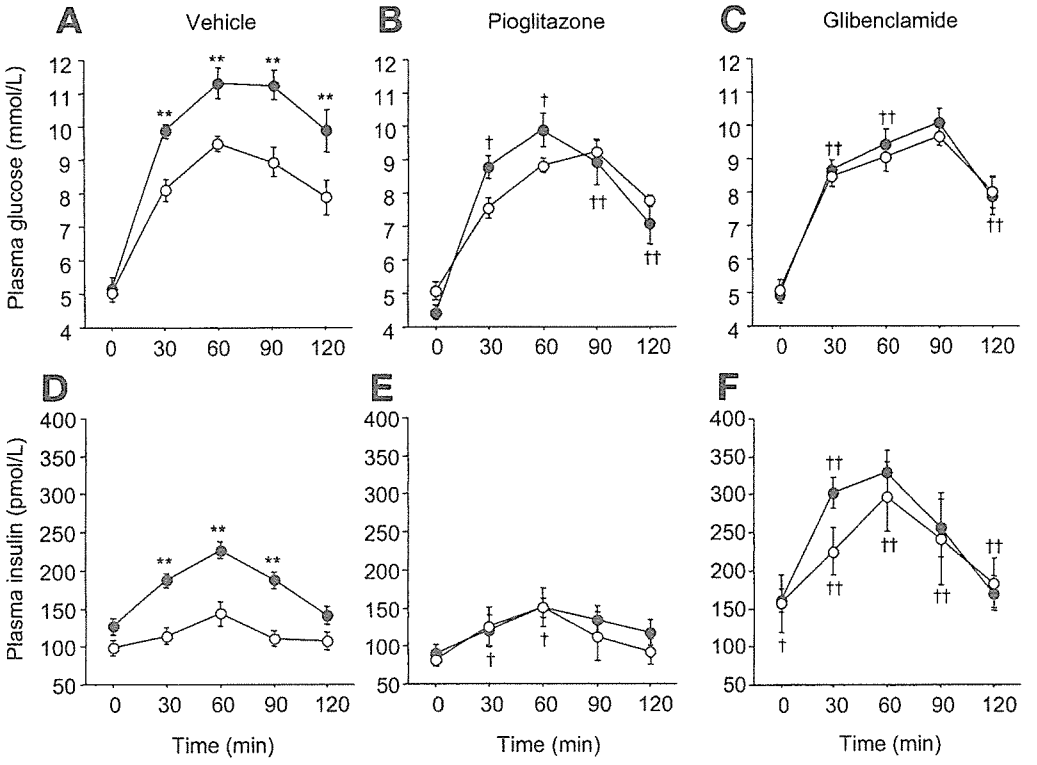

FIG. 1. Time courses in blood glucose (*A–C*) and plasma insulin (*D–F*) concentrations during OGTT. Data are mean ± SE. *A* and *D*: ○, LETO-VEH; ●, OLETF-VEH. *B* and *E*: ○, LETO-PIO; ●, OLETF-PIO. *C* and *F*: ○, LETO-GLIB; ●, OLETF-GLIB. **$P < 0.01$ vs. corresponding LETO groups. †$P < 0.05$, ††$P < 0.01$ vs. corresponding vehicle-treated groups.

plasma insulin concentrations, while no significant difference was observed in plasma glucose concentrations or indexes of lipid metabolism. In contrast, when compared with the OLETF-VEH group, the OLETF-GLIB group had higher body weight and left ventricular weight while no significant difference was observed in plasma glucose, insulin concentrations, or indexes of lipid metabolism.

OGTT. Figure 1 plots the plasma glucose and insulin concentrations during the OGTT. The increase of plasma glucose and insulin in response to oral glucose was more pronounced in the OLETF-VEH group than in the LETO-VEH group ($P < 0.01$ for each). Treatment with pioglitazone suppressed the increase of plasma glucose and insulin in the OLETF rats ($P < 0.01$ and $P < 0.05$ for each, respectively), resulting in no significant difference between the OLETF-PIO group and the LETO-PIO group. Treatment with glibenclamide also suppressed the increase of plasma glucose in the OLETF rats ($P < 0.01$). However, the treatment rather enhanced the increase of plasma insulin ($P < 0.05$).

Cardiac HSP72 expression and PI3 kinase dependence. Figure 2 depicts the cardiac HSP72 expression at 24 h after each thermo treatment in vehicle-treated rats. Hyperthermia induced HSP72 expression in both the LETO-VEH and the OLETF-VEH groups ($P < 0.01$ and $P < 0.05$, respectively). However, the levels of expression in OLETF-VEH group was less when compared with that in the LETO-VEH group ($P < 0.01$). The pretreatment with wortmannin inhibited the expression of HSP72 specifically in the LETO-VEH group ($P < 0.01$), resulting in no significant difference between the LETO-VEH group and the OLETF-VEH group.

Cardiac Akt phosphorylation and PI3 kinase dependence. Figure 3 depicts the phosphorylation of Akt at 1 h after each thermo treatment in vehicle-treated rats. The three representative bands for total Akt, phospho-Ser^{473}-

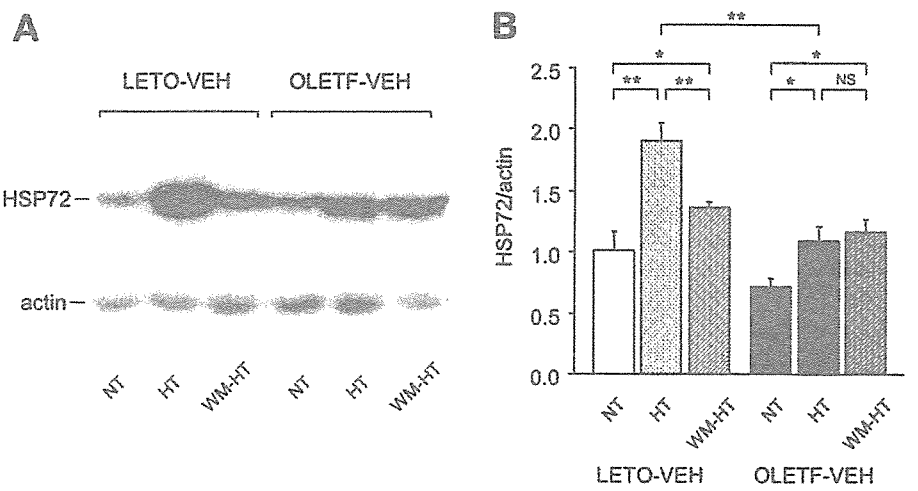

FIG. 2. Cardiac expression of HSP72 in LETO-VEH and OLETF-VEH groups. The heart was isolated 24 h after each thermo treatment. Representative immunoblot bands (*A*) and quantification of the ratio of HSP72 to actin (*B*). $n = 4$ for each group. Data are means ± SE. HT, hyperthermia; NT, normothermia; WM-HT, wortmannin pretreatment followed by HT. *$P < 0.05$, **$P < 0.01$.

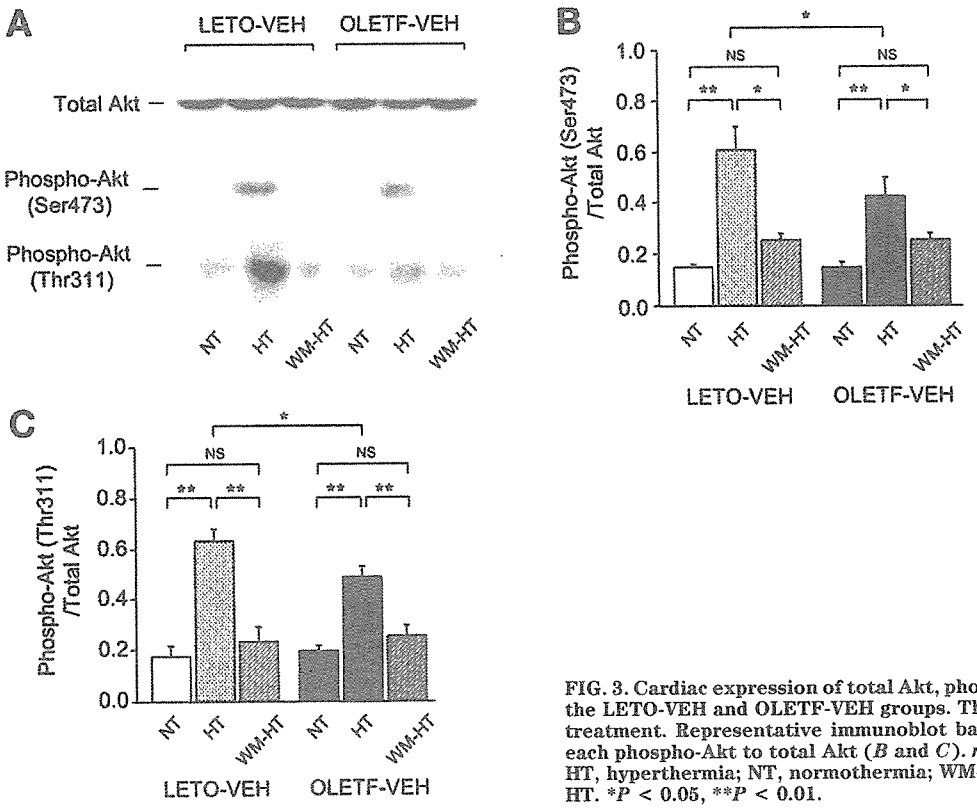

FIG. 3. Cardiac expression of total Akt, phospho-Ser^{473}-Akt, and phospho-Thr^{311}-Akt in the LETO-VEH and OLETF-VEH groups. The heart was isolated 1 h after each thermo treatment. Representative immunoblot bands (*A*) and quantification of the ratio of each phospho-Akt to total Akt (*B* and *C*). $n = 4$ for each group. Data are means ± SE. HT, hyperthermia; NT, normothermia; WM-HT, wortmannin pretreatment followed by HT. *$P < 0.05$, **$P < 0.01$.

Akt, and phospho-Thr^{311}-Akt are shown. Hyperthermia induced Akt phosphorylation in both the LETO-VEH and the OLETF-VEH groups ($P < 0.01$ for each). However, phosphorylation in the OLETF-VEH group was less when compared with that in the LETO-VEH group ($P < 0.05$). The pretreatment with wortmannin inhibited the Akt phosphorylation in both groups ($P < 0.05$ for each).

Reperfusion-induced left ventricular functional recovery. Figure 4*A* and *B* illustrate the serial changes in LVDP during the experimental period in the LETO-VEH and the OLETF-VEH groups. LVDP, heart rate, and CPP did not show a significant difference among the four experimental groups during the baseline period (data not shown). During no-flow global ischemia, LVDP decreased rapidly to zero. Hyperthermia, when compared with normothermia, improved left ventricular functional recovery in the LETO-VEH group ($P < 0.05$). However, the improvement did not reach statistical significance in the OLETF-VEH group (Fig. 4*A*). The improvement induced by hyperthermia in the LETO-VEH group was almost suppressed by the pretreatment with wortmannin (Fig. 4*B*). Figure 4*C* shows the amount of creatine kinase released during the 30 min of reperfusion period, which was greater in the OLETF-VEH group than in the LETO-VEH group ($P < 0.05$). Hyperthermia reduced the amount of released creatine kinase in the LETO-VEH group ($P < 0.05$), but the reduction did not reach statistical significance in the OLETF-VEH group. The pretreatment with wortmannin diminished the hyperthermia-induced reduction of released creatine kinase observed for the LETO-VEH group.

Effects of treatment with pioglitazone or glibenclamide on cardiac HSP72 expression. Figure 5 shows the effects of treatment with pioglitazone or glibenclamide on the expression of cardiac HSP72. Treatment with pioglitazone or glibenclamide did not influence the expression of HSP72 in the LETO groups. The observed depressed expression of HSP72 induced by hyperthermia in the OLETF-VEH group compared that in the LETO-VEH group ($P < 0.01$) was restored by treatment with pioglitazone. In contrast, treatment with glibenclamide resulted in failure to restore HSP72 expression.

Effects of pioglitazone treatment on Akt phosphorylation. Figure 6 depicts the effects of treatment with pioglitazone on Akt phosphorylation at 1 h after hyperthermia application. Treatment with pioglitazone restored Akt phosphorylation in the OLETF-VEH group, resulting in no significant difference between the LETO-PIO group and the OLETF-PIO group. The hyperthermia-induced Akt phosphorylation was suppressed by the pretreatment with wortmannin.

Effects of treatment with pioglitazone or glibenclamide on reperfusion-induced left ventricular functional recovery. Figure 7*A* and *B* illustrate the serial changes in LVDP during the experimental period. LVDP, heart rate, and CPP did not show a significant difference among the four experimental groups during the baseline period (data not shown). During no-flow global ischemia, LVDP decreased rapidly to zero. Hyperthermia improved left ventricular functional recovery in the LETO-PIO group and the OLETF-PIO group ($P < 0.01$ for each), although the improvement was more pronounced in the LETO-PIO group than that in the OLETF-PIO group ($P < 0.05$, Fig. 7*A*). In contrast, hyperthermia improved left ventricular functional recovery in the LETO-GLIB group ($P < 0.05$) but not in the OLETF-GLIB group (Fig. 7*B*). As shown in Fig. 7*C*, hyperthermia resulted in comparable levels of released creatine kinase between the LETO-PIO and the OLETF-PIO groups. However, hyperthermia did not reduce the amount of released creatine kinase in the OLETF-GLIB group.

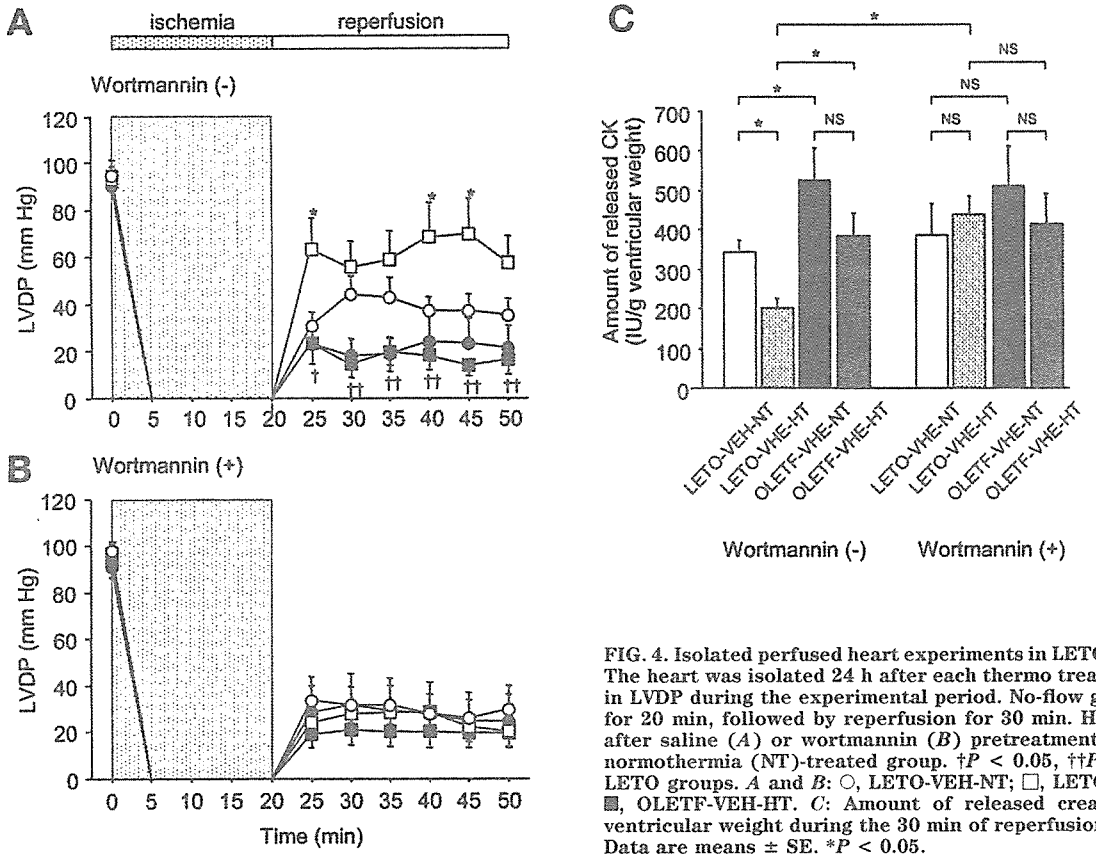

FIG. 4. Isolated perfused heart experiments in LETO-VEH and OLETF-VEH groups. The heart was isolated 24 h after each thermo treatment. *A* and *B*: Serial changes in LVDP during the experimental period. No-flow global ischemia was introduced for 20 min, followed by reperfusion for 30 min. Hyperthermia (HT) was applied after saline (*A*) or wortmannin (*B*) pretreatment. **P* < 0.05 vs. corresponding normothermia (NT)-treated group. †*P* < 0.05, ††*P* < 0.01 vs. the corresponding LETO groups. *A* and *B*: ○, LETO-VEH-NT; □, LETO-VEH-HT; ●, OLETF-VEH-NT; ■, OLETF-VEH-HT. *C*: Amount of released creatine kinase (CK) relative to ventricular weight during the 30 min of reperfusion period. *n* = 7 for each group. Data are means ± SE. **P* < 0.05.

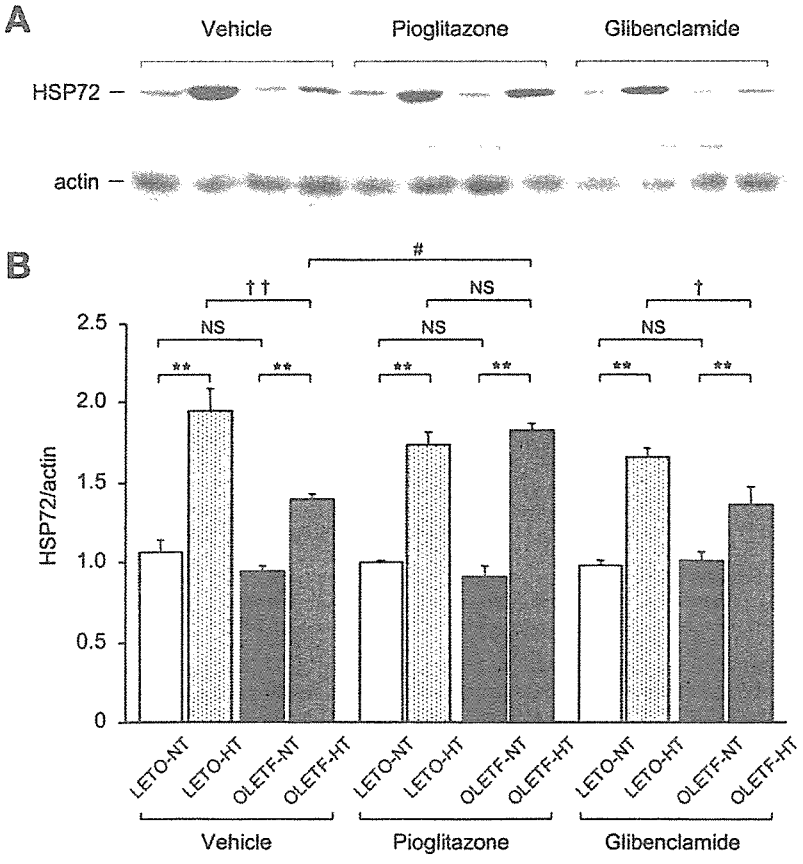

FIG. 5. Effects of pioglitazone or glibenclamide treatment on cardiac HSP72 expression. The heart was isolated 24 h after each thermo treatment. Representative immunoblot bands (*A*) and quantification of the ratio of HSP72 to actin (*B*). *n* = 4 for each group. Data are means ± SE. HT, hyperthermia; NT, normothermia. ***P* < 0.01 vs. corresponding NT-treated groups; †*P* < 0.05, ††*P* < 0.01 vs. corresponding LETO groups; #*P* < 0.05 vs. vehicle-treated group.

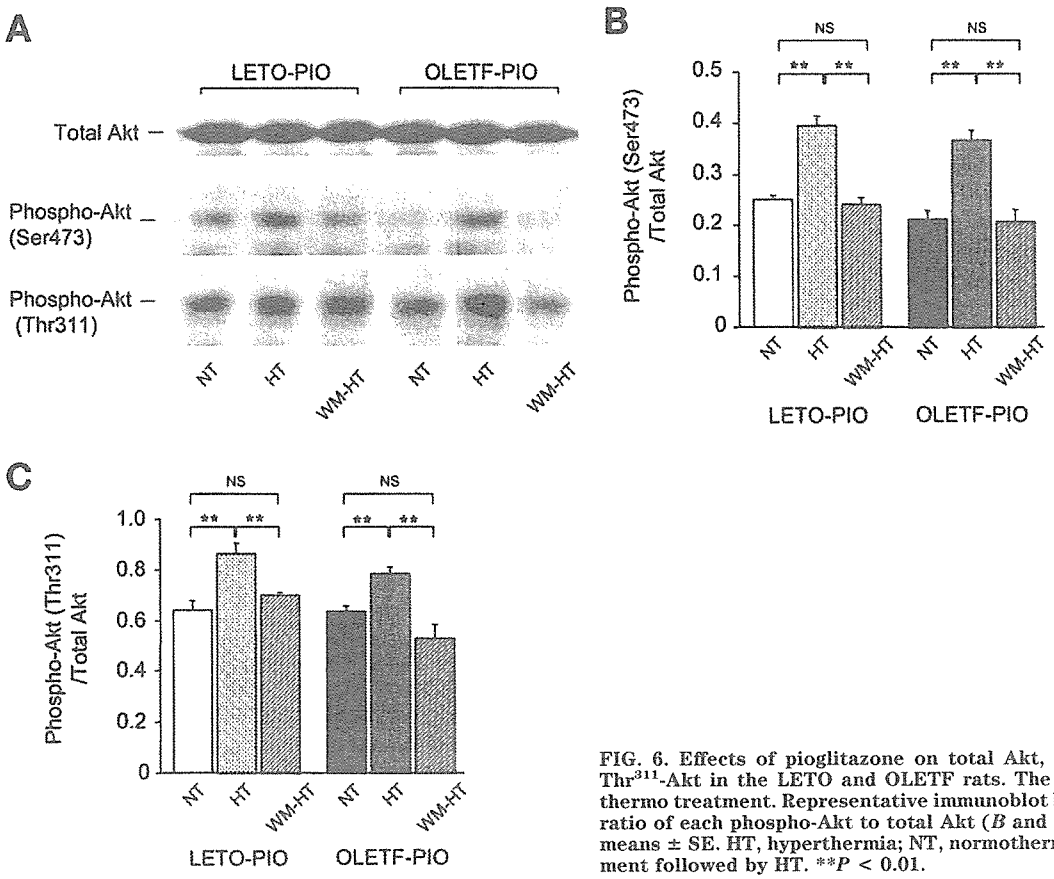

FIG. 6. Effects of pioglitazone on total Akt, phospho-Ser^{473}-Akt, and phospho-Thr^{311}-Akt in the LETO and OLETF rats. The heart was isolated 1 h after each thermo treatment. Representative immunoblot bands (*A*) and quantification of the ratio of each phospho-Akt to total Akt (*B* and *C*). $n = 4$ for each group. Data are means ± SE. HT, hyperthermia; NT, normothermia; WM-HT, wortmannin pretreatment followed by HT. $^{**}P < 0.01$.

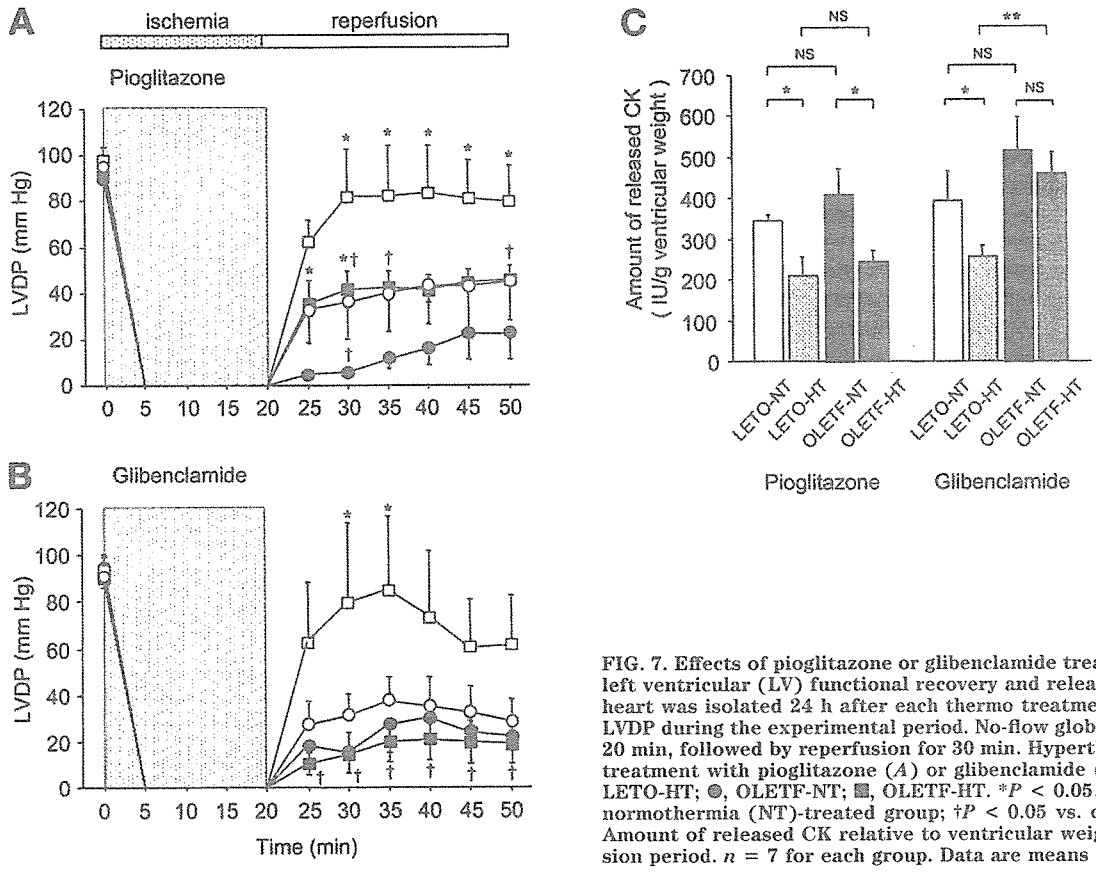

FIG. 7. Effects of pioglitazone or glibenclamide treatment on reperfusion-induced left ventricular (LV) functional recovery and released creatine kinase (CK). The heart was isolated 24 h after each thermo treatment. *A* and *B*: Serial changes in LVDP during the experimental period. No-flow global ischemia was introduced for 20 min, followed by reperfusion for 30 min. Hyperthermia (HT) was applied after treatment with pioglitazone (*A*) or glibenclamide (*B*). *A* and *B*: ○, LETO-NT; □, LETO-HT; ●, OLETF-NT; ■, OLETF-HT. $^{*}P < 0.05$, $^{**}P < 0.01$ vs. corresponding normothermia (NT)-treated group; $^{\dagger}P < 0.05$ vs. corresponding LETO group. *C*: Amount of released CK relative to ventricular weight during the 30-min reperfusion period. $n = 7$ for each group. Data are means ± SE. $^{*}P < 0.05$, $^{**}P < 0.01$.

DISCUSSION

The core findings of the present study are as follows. *1*) In response to hyperthermia, the Akt activation depending on PI3 kinase was necessary for cardiac HSP72 expression. *2*) Hyperthermia-induced Akt activation and HSP72 expression was depressed in OLETF rat hearts. *3*) Pioglitazone but not glibenclamide improved insulin sensitivity in OLETF rats, which was associated with the restoration of Akt activation and HSP72 expression. *4*) In isolated perfused heart experiments, reperfusion-induced left ventricular functional recovery was suppressed in OLETF rat hearts, which was restored by treatment with pioglitazone but not glibenclamide.

In the present study, we used OLETF rats, which have been established as an animal model of type 2 diabetes, characterized by late onset of hyperglycemia (after 20 weeks of age), mild course of diabetes, and conversion to insulin-dependent diabetes after ~40 weeks of age (22,23). In our protocol, 12-week-old rats were introduced to receive oral pioglitazone or glibenclamide for 4 weeks. At 16 weeks, when compared with corresponding control LETO rats, while plasma glucose concentrations were not significantly different, plasma insulin concentrations were higher in OLETF rats. In addition, during OGTT, increases of plasma glucose and insulin concentrations were greater in OLETF rats. Thus, vehicle-treated OLETF rats of 16 weeks of age can be regarded as an insulin-resistant model but not a type 2 diabetic model. As shown in Table 1 and Fig. 1, in OLETF rats, both pioglitazone and glibenclamide suppressed the increase of plasma glucose during OGTT. However, their effects on plasma insulin were strikingly different. While pioglitazone improved insulin sensitivity, glibenclamide rather worsened it. These findings suggest that the differences of our observations between pioglitazone-treated and glibenclamide-treated OLETF rats may be, at least in part, due to differed alteration in insulin sensitivity despite the similar levels of plasma glucose.

Information is very limited with respect to the impact of insulin resistance and type 2 diabetes on HSP72 expression. In the study using human subjects, Kurucz et al. (9) provided the first evidence of decreased expression of the HSP72 mRNA in skeletal muscle from patients with type 2 diabetes, with this reduction being correlated with some markers of insulin resistance. Consistently, Bruce et al. (24) demonstrated that intramuscular HSP72 and heme oxygenase-1 mRNA were reduced in patients with type 2 diabetes. The authors reported the more convinced correlation between a reduction in HSP72 mRNA with insulin resistance (24). However, these clinical studies evaluated the HSP72 mRNA expression only in skeletal muscle and did not provide the underlying mechanism. In this regard, we have focused on PI3 kinase–dependent Akt phosphorylation as a triggering mechanism for hyperthermia-induced HSP72 expression. In fact, we have recently reported that transient activation of Akt in a PI3 kinase–dependent manner is required for hyperthermia-induced HSP72 expression and that streptozotocin (STZ)-induced diabetic rat heart showed an attenuation of this response, resulting in depressed HSP72 expression (19). Because insulin supplementation restored these abnormalities, we proposed insulin deficiency is a predominant etiology for depressed PI3 kinase–dependent Akt activation in response to hyperthermia in STZ-induced diabetic heart (19). It is noteworthy that OLETF rats, characterized by insulin resistance, also showed attenuated PI3 kinase–dependent Akt phosphorylation in response to hyperthermia in the present study. Although it appears difficult to explain the disparity, these two animal models may have common pathogenesis in a sense. The cardiac muscles in STZ-induced diabetic rat cannot utilize insulin due to insulin deficiency while those in OLETF rat cannot effectively utilize insulin because of insulin resistance. This hypothesis may be supported by the combination of our previous (19) and present observations; that is, both insulin supplementation in STZ-induced diabetic rat (19) and improvement in insulin resistance in OLETF rat by pioglitazone in the present study could restore the PI3 kinase–dependent Akt phosphorylation and resultant HSP72 expression.

Thiazolidinediones, including pioglitazone, are synthetic PPAR-γ agonists, acting as insulin sensitizers (14,15). In the last few years, it has been reported numerically that the therapeutic benefits of PPAR-γ agonists may reach far beyond their use as insulin sensitizers (25). It is noteworthy that pioglitazone reportedly leads to increased expression of HSP72 in the gastric mucosa in acetic-acid gastric ulcers in association with promoting ulcer healing (26). Regarding myocardial ischemia/reperfusion injury, chronic troglitazone administration improved left ventricular functional recovery and increased net myocardial lactate uptake, indicating that troglitazone enhances myocardial carbohydrate oxidation (27). It was also reported that rosiglitazone attenuated the increase in caspase-3 activity and apoptotic cell death (28). More recently, using Zucker diabetic fatty (ZDF) rats, Yue et al. (29) reported that oral rosiglitazone administration for 8 days reduced ischemia/reperfusion-induced infarct size and apoptosis, which was in association with an improvement of insulin sensitivity. It is noteworthy that Akt phosphorylation in ZDF rat heart subjected to ischemia/reperfusion was enhanced by rosiglitazone. In their experiments, the Akt phosphorylation might induce cell surviving cascade against apoptosis. Thus, the restoration of Akt phosphorylation in response to hyperthermia observed in pioglitazone-treated OLETF rats may be due to diverse effects derived from the activation of PPAR-γ.

Limitations. There are several reservations in the present study. First, we discussed PI3 kinase–dependent Akt phosphorylation as a predominant signal for hyperthermia-induced HSP72 overexpression. However, in either OLETF or LETO rats, while the pretreatment with wortmannin completely inhibited Akt phosphorylation by hyperthermia (Fig. 3), it resulted in failure to completely suppress the HSP72 expression (Fig. 2). These observations suggest the working of operative mechanisms other than activation of PI3 kinase–dependent Akt activation for hyperthermia-induced HSP72 expression, which should be clarified in a future study. Second, our experiments could not establish whether pioglitazone-induced HSP72 expression improves reperfusion-induced cardiac functional recovery. To answer this issue appropriately, specific inhibition of expression of the HSP72 gene by, for instance, intracoronary injection of antisense HSP72 oligonucleotide, will be required. Third, in the clinical setting, it appears impossible to introduce the patients to temperatures as high as 43°C. It should be determined whether other HSP72 inducers, including GGA (5,6), lead to similar results. Fourth, our experiments were not performed in a single session under the same conditions. For instance, the absolute ratio of phospho-Akt/total Akt that appears in Fig. 3 is difficult to compare with what appears in Fig. 6.

Finally, the amount of released creatine kinase did not correlate well with the LVDP recovery during reperfusion period (Figs. 4 and 7). Especially in hyperthermia-treated OLETF rat hearts, the reperfusion-induced left ventricular functional recovery appeared to be depressed compared with the reduction in released creatine kinase. The finding suggests the complicated functional damage of OLETF rat hearts in response to ischemia/reperfusion, which was not reflected as released creatine kinase.

Conclusions. Our results suggest that PI3 kinase–dependent Akt activation in response to hyperthermia, an essential signal for HSP72 expression, at least in part, is depressed in the heart of insulin-resistant OLETF rats, and the results also suggest that restorations of HSP72 expression and tolerance against ischemia/reperfusion injury with pioglitazone in OLETF heart might be due to a restoration of impaired PI3 kinase–dependent Akt activation in response to hyperthermia.

ACKNOWLEDGMENTS

This study was supported in part by a grant-in-aid 17590756 (T.S.) from the Japanese Ministry of Education, Science and Culture.

REFERENCES

1. Benjamin IJ, McMillan DR: Stress (heat shock) proteins: molecular chaperones in cardiovascular biology and disease. *Circ Res* 83:117–132, 1998
2. Williams RS, Benjamin IJ: Protective responses in the ischemic myocardium. *J Clin Invest* 106:813–818, 2000
3. Latchman DS: Heat shock proteins and cardiac protection. *Cardiovasc Res* 51:637–646, 2001
4. Marber MS, Mestril R, Chi SH, Sayen MR, Yellon DM, Dillmann WH: Overexpression of the rat inducible 70-kD heat stress protein in a transgenic mouse increases the resistance of the heart to ischemic injury. *J Clin Invest* 95:1446–1456, 1995
5. Ooie T, Takahashi N, Saikawa T, Nawata T, Arikawa M, Yamanaka K, Hara M, Shimada T, Sakata T: Single oral dose of geranylgeranylacetone induces heat-shock protein 72 and renders protection against ischemia/reperfusion injury in rat heart. *Circulation* 104:1837–1843, 2001
6. Yamanaka K, Takahashi N, Ooie T, Kaneda K, Yoshimatsu H, Saikawa T: Role of protein kinase C in geranylgeranylacetone-induced expression of heat-shock protein 72 and cardioprotection in the rat heart. *J Mol Cell Cardiol* 35:785–794, 2003
7. Shinohara T, Takahashi N, Ooie T, Ichinose M, Hara M, Yonemochi H, Saikawa T, Yoshimatsu H: Estrogen inhibits hyperthermia-induced expression of heat-shock protein 72 and cardioprotection against ischemia/reperfusion injury in female rat heart. *J Mol Cell Cardiol* 37:1053–1061, 2004
8. Zhu Z, Takahashi N, Ooie T, Shinohara T, Yamanaka K, Saikawa T: Oral administration of geranylgeranylacetone blunts the endothelial dysfunction induced by ischemia and reperfusion in the rat heart. *J Cardiovasc Pharmacol* 45:555–562, 2005
9. Kurucz I, Morva A, Vaag A, Eriksson KF, Huang X, Groop L, Koranyi L: Decreased expression of heat shock protein 72 in skeletal muscle of patients with type 2 diabetes correlates with insulin resistance. *Diabetes* 51:1102–1109, 2002
10. Ooie T, Kajimoto M, Takahashi N, Shinohara T, Taniguchi Y, Kouno H, Wakisaka O, Yoshimatsu H, Saikawa T: Effects of insulin resistance on geranylgeranylacetone-induced expression of heat shock protein 72 and cardioprotection in high-fat diet rats. *Life Sci* 77:869–881, 2005
11. Folli F, Saad MJ, Backer JM, Kahn CR: Regulation of phosphatidylinositol 3-kinase activity in liver and muscle of animal models of insulin-resistant and insulin-deficient diabetes mellitus. *J Clin Invest* 92:1787–1794, 1993
12. Saad MJ, Folli F, Kahn JA, Kahn CR: Modulation of insulin receptor, insulin receptor substrate-1, and phosphatidylinositol 3-kinase in liver and muscle of dexamethasone-treated rats. *J Clin Invest* 92:2065–2072, 1993
13. Abel ED: Myocardial insulin resistance and cardiac complications of diabetes. *Curr Drug Targets Immune Endocr Metabol Disord* 5:219–226, 2005
14. Kobayashi M, Iwanishi M, Egawa K, Shigeta Y: Pioglitazone increases insulin sensitivity by activating insulin receptor kinase. *Diabetes* 41:476–483, 1992
15. Hayakawa T, Shiraki T, Morimoto T, Shii K, Ikeda H: Pioglitazone improves insulin signaling defects in skeletal muscle from Wistar fatty (fa/fa) rats. *Biochem Biophys Res Commun* 223:439–444, 1996
16. Fujio Y, Nguyen T, Wencker D, Kitsis RN, Walsh K: Akt promotes survival of cardiomyocytes in vitro and protects against ischemia-reperfusion injury in mouse heart. *Circulation* 101:660–667, 2000
17. Konishi H, Matsuzaki H, Tanaka M, Ono Y, Tokunaga C, Kuroda S, Kikkawa U: Activation of RAC-protein kinase by heat shock and hyperosmolarity stress through a pathway independent of phosphatidylinositol 3-kinase. *Proc Natl Acad Sci U S A* 93:7639–7643, 1996
18. Shaw M, Cohen P, Alessi DR: The activation of protein kinase B by H_2O_2 or heat shock is mediated by phosphoinositide 3-kinase and not by mitogen-activated protein kinase-activated protein kinase-2. *Biochem J* 336:241–246, 1998
19. Shinohara T, Takahashi N, Ooie T, Hara M, Shigematsu S, Nakagawa M, Yonemochi H, Saikawa T, Yoshimatsu H: Phosphatidylinositol 3-kinase-dependent activation of Akt, an essential signal for hyperthermia-induced heat shock protein 72, is attenuated in the streptozotocin-induced diabetic heart. *Diabetes* 55:1307–1315, 2006
20. Bradford MM: A rapid and sensitive method for quantitation of microgram quantities of protein utilizing the principle of protein-dye binding. *Anal Biochem* 72:248–254, 1976
21. Mekhfi H, Veksler V, Mateo P, Maupoil V, Rochette L, Ventura-Clapier R: Creatine kinase is the main target of reactive oxygen species in cardiac myofibrils. *Circ Res* 78:1016–1027,1996
22. Kawano K, Hirashima T, Mori S, Saitoh Y, Kurosumi M, Natori T: Spontaneous long-term hyperglycemic rat with diabetic complications: Otsuka Long-Evans Tokushima Fatty (OLETF) strain. *Diabetes* 41:1422–1428, 1992
23. Sato T, Asahi Y, Toide K, Nakayama N: Insulin resistance in skeletal muscle of the male Otsuka Long-Evans Tokushima Fatty rat, a new model of NIDDM. *Diabetologia* 38:1033–1041, 1995
24. Bruce CR, Carey AL, Hawley JA, Febbraio MA: Intramuscular heat shock protein 72 and heme oxygenase-1 mRNA are reduced in patients with type 2 diabetes: evidence that insulin resistance is associated with a disturbed antioxidant defense mechanism *Diabetes* 52:2338–2345, 2003
25. Abdelrahman M, Sivarajah A, Thiemermann C: Beneficial effects of PPAR-γ ligands in ischemia-reperfusion injury, inflammation and shock. *Cardiovasc Res* 65:772–781, 2005
26. Konturek PC, Brzozowski T, Kania J, Konturek SJ, Kwiecien S, Pajdo R, Hahn EG: Pioglitazone, a specific ligand of peroxisome proliferator-activated receptor-gamma, accelerates gastric ulcer healing in rat. *Eur J Pharmacol* 472:213–220, 2003
27. Zhu P, Lu L, Xu Y, Schwartz GG: Troglitazone improves recovery of left ventricular function after regional ischemia in pigs. *Circulation* 101:1165–1171, 2000
28. Liu HR, Tao L, Gao E, Lopez BL, Christopher TA, Willette RN, Ohlstein EH, Yue TL, Ma XL: Anti-apoptotic effects of rosiglitazone in hypercholesterolemic rabbits subjected to myocardial ischemia and reperfusion. *Cardiovasc Res* 62:135–144, 2004
29. Yue TL, Bao W, Gu JL, Cui J, Tao L, Ma XL, Ohlstein EH, Jucker BM: Rosiglitazone treatment in Zucker diabetic Fatty rats is associated with ameliorated cardiac insulin resistance and protection from ischemia/reperfusion-induced myocardial injury. *Diabetes* 54:554–562, 2005

THE JOURNAL OF BIOLOGICAL CHEMISTRY VOL. 281, NO. 39, pp. 28657–28665, September 29, 2006

Constitutive GDP/GTP Exchange and Secretion-dependent GTP Hydrolysis Activity for Rab27 in Platelets*

Received for publication, April 5, 2006, and in revised form, June 19, 2006 Published, JBC Papers in Press, July 31, 2006, DOI 10.1074/jbc.M603227200

Hirokazu Kondo[‡], Ryutaro Shirakawa[‡1], Tomohito Higashi[‡1], Mitsunori Kawato[‡], Mitsunori Fukuda[§¶], Toru Kita[‡], and Hisanori Horiuchi[‡2]

From the [‡]Department of Cardiovascular Medicine, Graduate School of Medicine, Kyoto University, Kyoto 606-8507, the [§]Fukuda Initiative Research Unit, RIKEN, Wako, Saitama 351-0198, and the [¶]Laboratory of Membrane Trafficking Mechanisms, Department of Developmental Biology and Neurosciences, Graduate School of Life Sciences, Tohoku University, Aobayama, Aoba-ku, Sendai, Miyagi 980-8578, Japan

We have previously demonstrated that Rab27 regulates dense granule secretion in platelets. Here, we analyzed the activation status of Rab27 using the thin layer chromatography method analyzing nucleotides bound to immunoprecipitated Rab27 and the pull-down method quantifying Rab27 bound to the GTP-Rab27-binding domain (synaptotagmin-like protein (Slp)-homology domain) of its specific effector, Slac2-b. We found that Rab27 was predominantly present in the GTP-bound form in unstimulated platelets due to constitutive GDP/GTP exchange activity. The GTP-bound Rab27 level drastically decreased due to enhanced GTP hydrolysis activity upon granule secretion. In permeabilized platelets, increase of Ca^{2+} concentration induced dense granule secretion with concomitant decrease of GTP-Rab27, whereas in non-hydrolyzable GTP analogue GppNHp (β-γ-imidoguanosine 5′-triphosphate)-loaded permeabilized platelets, the GTP (GppNHp)-Rab27 level did not decrease upon the Ca^{2+}-induced secretion. These data suggested that GTP hydrolysis of Rab27 was not necessary for inducing the secretion. Taken together, Rab27 is maintained in the active status in unstimulated platelets, which could function to keep dense granules in a preparative status for secretion.

In eukaryotic cells, transport between distinct organelles is performed through vesicle trafficking. The final step of vesicle docking/fusion with target membrane is mediated by *trans*-soluble *N*-ethylmaleimide-sensitive factor attachment protein receptor (SNARE)[3] complex bridging a vesicle and its target membrane (1). One of the key regulators for the SNARE complex formation is Rab GTPase (2, 3). So far, more than 60 members of Rab GTPases are identified in mammals, and they play critical roles in the specific transport pathways (2–4). Like other GTPases, the activity of Rab is regulated by its GDP/GTP cycle. Rab proteins have GTP-bound active and GDP-bound inactive forms. The activation process is performed by GDP/GTP exchange mediated by the GDP/GTP exchange factor. GTP-bound Rabs execute their function by interaction with effector proteins. Then, GTP-Rab is inactivated into GDP-Rab by GTP hydrolysis that is mediated by the intrinsic GTPase activity and its enhancer, GTPase-activating protein. Furthermore, the Rab family has a unique regulatory protein named Rab GDP dissociation inhibitor (RabGDI), which extracts GDP-Rab from membrane into cytosol by forming a 1:1 complex and inhibits GDP/GTP exchange (3). RabGDI accompanies Rabs in cytosol to the correct organelles, where they are reactivated by the function of GDI dissociation factor (5–8).

Although elucidation of the regulatory mechanism of the GDP/GTP cycle is crucial for understanding the functional mechanism of Rab GTPases, it has not been extensively investigated so far. Small GTPases belonging to Ras and Rho families are predominantly present in the GDP-bound forms under resting conditions and are transiently activated into GTP-bound forms upon stimulation (9), indicating that these GTPases function as "switches" that transduce extracellular signals. For Rab GTPases, most of Rab5, a regulator of endocytic pathway (10, 11), is in the GDP-bound form in unstimulated NR6 cells, and more than half of Rab5 rapidly and transiently becomes the GTP-bound active form upon epidermal growth factor stimulation (12). On the other hand, ~80% of Rab3D is in the GTP-bound form in unstimulated pancreatic acini (13). Since these two results are quite opposite, it is unclear whether RabGTPases are present in its GTP-bound or GDP-bound form. Furthermore, it is not known whether the activation status of other Rab GTPases is altered upon stimulation, like Rab5.

Rab27 is composed of two isoforms, Rab27A and Rab27B, that share ~70% identical amino acid residues (14–16). Accumulating evidence revealed that Rab27 is a general regulator for regulated exocytosis in non-neuronal cells, such as lytic granule

* This work was supported by Ministry of Education, Culture, Sports, Science, and Technology Research Grants, Japan, and by Health and Labor Sciences Research Grant for Cardiovascular Research from the Ministry of Health Labor and Welfare, Japan. This study was also supported in part by grants from the Takeda Science Foundation, Japan Heart Foundation Young Investigator's Research Grant and Japan Heart Foundation Pfizer Japan Inc. Grant for Research on Cardiovascular Disease. The costs of publication of this article were defrayed in part by the payment of page charges. This article must therefore be hereby marked "*advertisement*" in accordance with 18 U.S.C. Section 1734 solely to indicate this fact.

[1] Recipients of the Japan Society for the Promotion of Science Research Fellowship for Young Scientists.

[2] To whom correspondence should be addressed. Tel.: 81-75-751-3778; Fax: 81-75-751-3203; E-mail: horiuchi@kuhp.kyoto-u.ac.jp.

[3] The abbreviations used are: SNARE, soluble *N*-ethylmaleimide-sensitive factor attachment protein receptor; GDI, GDP dissociation inhibitor; Slp, synaptotagmin-like protein; SHD, synaptotagmin-like protein homology domain; Slac2, synaptotagmin-like protein homologue lacking C2 domains; GST, glutathione *S*-transferase; NEM, *N*-ethylmaleimide; GTPγS, guanosine 5′-3-*O*-(thio)triphosphate; GppNHp, β-γ-imidoguanosine 5′-triphosphate.

secretion in cytotoxic T cells (17, 18), insulin secretion in pancreatic β-cells (19), and histamine-containing granule secretion in mast cells (20, 21). Rab27 also regulates melanosome traffic along actin cytoskeleton in melanocytes (22–25).

Dense granules in platelets contain self-agonists such as ADP and serotonin. Secreted ADP and serotonin play important roles for positive feedback activation of platelets at the site of thrombus formation (26, 27). We have demonstrated that Rab27 regulates the secretion in platelets by showing that the addition of non-prenylated Rab27A or Rab27B purified from *Escherichia coli* specifically inhibited the secretion in an assay using permeabilized platelets, possibly due to sequestering its putative effector molecules (28). We have identified a Rab27 effector in platelet cytosol as Munc13-4 (28). Munc13-4 is a non-neuronal homologue of Munc13-1, an essential priming factor in neuronal secretion.

In addition to Munc13-4, eight Rab27 effector molecules have been identified. Although a GTP-Rab27-binding minimal domain of Munc13-4 has not been determined, these eight molecules contain a common GTP-Rab27-binding structure named synaptotagmin-like protein (Slp)-homology domains (SHD) ~100 amino acid long at their N-terminal ends (16). These eight molecules are classified into two groups: Slp1~5 containing two C2 calcium-binding domains and Slp-lacking C2 domains (Slac2)-a~c (16). Although some SHDs potentially bind other Rab proteins in addition to Rab27, SHD of Slac2-b is specific for GTP-Rab27 among 20 tested Rab GTPases (16, 29).

Here, to analyze the GDP/GTP-bound status of Rab27 in platelets, we utilized two assays, a GTP-Rab27 pull-down assay using SHD of Slac2-b and an assay using thin layer chromatography analyzing GDP/GTP associated with immunoprecipitated Rab27. By these two methods, we demonstrated that Rab27 in unstimulated platelets was predominantly in the GTP-bound form, a state that was maintained by constitutive GDP/GTP exchange activity. The GTP-bound form of Rab27 drastically decreased upon granule secretion, due to enhanced GTP hydrolysis activity that was secretion-dependent. Furthermore, we showed that GTP hydrolysis of Rab27 might not be required for the induction of secretion in platelets, namely hydrolysis would be a consequence of secretion.

EXPERIMENTAL PROCEDURES

Materials—Rabbit polyclonal anti-Rab27A (28) and -Rab27B (30) antibodies were generated using His_6-Rab27A and glutathione *S*-transferase (GST)-Rab27B as antigens, respectively. For Rab27 immunoprecipitation, we used both antibodies in combination. Mouse monoclonal anti-His_6 antibody was purchased from Sigma. Horseradish peroxidase-labeled anti-rabbit and anti-mouse IgG polyclonal antibodies were from Amersham Biosciences and used as secondary antibodies for Western blot analysis visualized by the enhanced chemiluminescence method (Amersham Biosciences). Streptolysin-O was from Dr. S. Bhakdi (Mainz University, Mainz, Germany) (31). [α-^{32}P]GTP (3,000 Ci/mmol), and [γ-^{32}P]GTP (3,000 Ci/mmol) were purchased from PerkinElmer Life Sciences, and [^{32}P]phosphorus (200 μCi/mmol) was from Amersham Biosciences. Unless otherwise specified, all the other chemicals including nucleotides, *N*-ethylmaleimide (NEM), and thrombin were purchased from Sigma.

cDNA encoding rat Rab27A was kindly provided by Dr. Y. Nozawa (Gifu International Institute of Biotechnology, Gifu, Japan) (14). Human Rab27B cDNA was cloned from the Marathon-Ready human bone marrow cDNA (Clontech) by PCR. SHD of Slac2-b (KIAA0624) (amino acids 1–79) was generated by PCR using KIAA0624 clone provided by Kazusa DNA Research Institute as a template. All the sequences of PCR products were confirmed by a 3100 genetic analyzer (Applied Biosystems). cDNAs were subcloned into the prokaryotic expression vector pDEST17 (Invitrogen) for His_6-tagged protein and pGEX-2T (Amersham Biosciences) for GST fusion proteins. These His_6-tagged and GST fusion proteins were produced in *E. coli* strain BL21 and purified according to the manufacturers' instructions. All the purified recombinant proteins were extensively dialyzed against Buffer A (50 mM HEPES/KOH, pH 7.2, 78 mM KCl, 4 mM $MgCl_2$, 0.2 mM $CaCl_2$, 2 mM EGTA, 1 mM dithiothreitol) and stored at −80 °C until use. Protein concentrations were determined by the Bradford method (Bio-Rad) or from the intensities of the bands in Coomassie Blue-stained SDS-PAGE gels using bovine serum albumin as a standard.

Platelet Dense Granule Secretion Assays—Freshly obtained washed platelets (5×10^7 platelets/assay, counted with the Coulter counter) were incubated with [^{3}H]serotonin (Amersham Biosciences) to allow uptake into dense core granules (~20,000 cpm/assay) followed by washing with Buffer A. For the assay using intact platelets, they were stimulated with 0.5 units/ml thrombin (Sigma) at 30 °C for the indicated periods, and secreted [^{3}H]serotonin was measured by a liquid scintillation counter (Beckman) after removing platelets by centrifugation. The secretion levels of [^{3}H]serotonin were expressed as percentages of the total [^{3}H]serotonin in the platelets before the final incubation.

The method of dense granule secretion assay using platelets permeabilized by streptolysin-O was described previously (28, 32–35). Briefly, plasma membrane of [^{3}H]serotonin-loaded platelets was permeabilized with streptolysin-O in Buffer A, where the calculated free Ca^{2+} concentration was ~20 nM (36). The permeabilized platelets were incubated with ATP, human platelet cytosol at 2.0 mg of proteins/ml, and tested materials at 4 °C for 15–30 min followed by further incubation at 30 °C for 3 min. Finally, the platelets were stimulated with 20 μM Ca^{2+} (36) at 30 °C for the indicated periods, and the reaction was stopped by the addition of ice-cold Buffer A containing 10 mM EGTA.

Assay Analyzing Specific Binding of SHD of Slac2-b with GTP-Rab27—Binding of SHD of Slac2-b with Rab27 was performed by affinity chromatography. First, a non-hydrolyzable GTP analogue, GTPγS, and GDP-bound His_6-Rab27A and His_6-Rab27B were prepared by incubation of these GTPases (0.2 μM) with 1 mM GTPγS and GDP in the presence of 4 mM $MgCl_2$ and 10 mM EDTA at 30 °C for 30 min followed by the addition of 15 mM $MgCl_2$ to quit the reaction as described (7). Then, GDP- and GTPγS-preloaded Rab27 (1 μg) was incubated with glutathione-Sepharose beads (Amersham Biosciences) coated with GST-SHD of Slac2-b at 4 °C for 1 h in Buffer A and washed three times with the same buffer. Bead-

associated His_6-Rab27 was analyzed by immunoblotting with anti-His_6 antibody.

GTP-Rab27 Pull-down Assay with GST-SHD of Slac2-b—The amount of GTP-bound Rab27 in platelets was measured by affinity pull-down using the SHD. The standard assay was as follows. Platelets isolated from freshly obtained whole blood were lysed in Buffer A containing 0.5% Triton X-100 and protease inhibitor mixture (P8340, Sigma) at 4 °C for 5 min followed by centrifugation at 300,000 × *g* for 5 min. This procedure completely extracted Rab27. Then, the supernatants were incubated with glutathione beads coated with 10 μg of GST-SHD at 4 °C for 30 min. The beads were washed three times with Buffer A containing 0.1% Triton X-100 and the protease inhibitor mixture, and bead-associated Rab27 was analyzed by immunoblotting with anti-Rab27 antibody. Densitometric analysis of appropriately exposed film was performed, and the signals were quantified using Image J 1.33u software (National Institutes of Health).

To calculate the ratio of GDP/GTP, the standards were produced as described previously (13). The same amount of aliquots of the Triton X-100 extract was incubated at 30 °C for 90 min in the presence of 10 mM EDTA and 4 mM $MgCl_2$ with 1 mM GppNHp (a non-hydrolyzable GTP analogue) or GDP followed by the addition of 15 mM $MgCl_2$ to quit the reaction and determination of GTP-bound Rab27 by the pull-down method. The amount of pulled down Rab27 in the platelet lysate after incubation with GppNHp was defined as 100%, and that with GDP was defined as 0%.

Evaluation of Nucleotide Bound to Rab27—Washed platelets (2×10^8 platelets/assay) were incubated with 300 μCi of [^{32}P]phosphorus (200 μCi/mmol; Amersham Biosciences) in Buffer B (138 mM NaCl, 2.9 mM KCl, 1.8 mM $CaCl_2$, 12 mM $NaHCO_3$, 0.49 mM $MgCl_2$, 5.5 mM glucose, 50 mM HEPES/KOH, pH 7.4) at 37 °C for 3 h. After the platelets were washed with Buffer B twice followed by incubation at 30 °C for 3 min, they were stimulated with 0.5 units/ml thrombin at 30 °C for 3 min. Then, platelets were lysed with Buffer A containing 0.5% Triton X-100 and the protease inhibitor mixture at 4 °C for 5 min. Supernatants after centrifugation were immunoprecipitated using anti-Rab27 antibodies at 4 °C for 30 min. Bound nucleotides were eluted in 25 μl of Buffer A containing 0.2% SDS, 10 mM EDTA, 1 mM GTP, and 1 mM GDP at 85 °C for 3 min. The samples (6 μl of each) were then spotted onto a polyethyleneimine-cellulose TLC plate (Merck) and developed for 90 min in 1 M $LiCl_2$ and 1 M formic acid. The plates were dried and placed at −80 °C for 36–48 h for autoradiography. Densitometric analysis of appropriately exposed film was performed, and the signals were quantified using Image J 1.33u software (National Institutes of Health).

Statistical Analysis—All values presented are means ± S.E. Student's *t* test was used in Fig. 7*A*. Values of $p < 0.05$ were considered statistically significant.

RESULTS

Characterization of the SHD of Slac2-b as the GTP-Rab27-interacting Domain—We first characterized the SHD of a Rab27-specific effector, Slac2-b. We examined whether GST-SHD specifically bound GTP-bound Rab27A and Rab27B, both

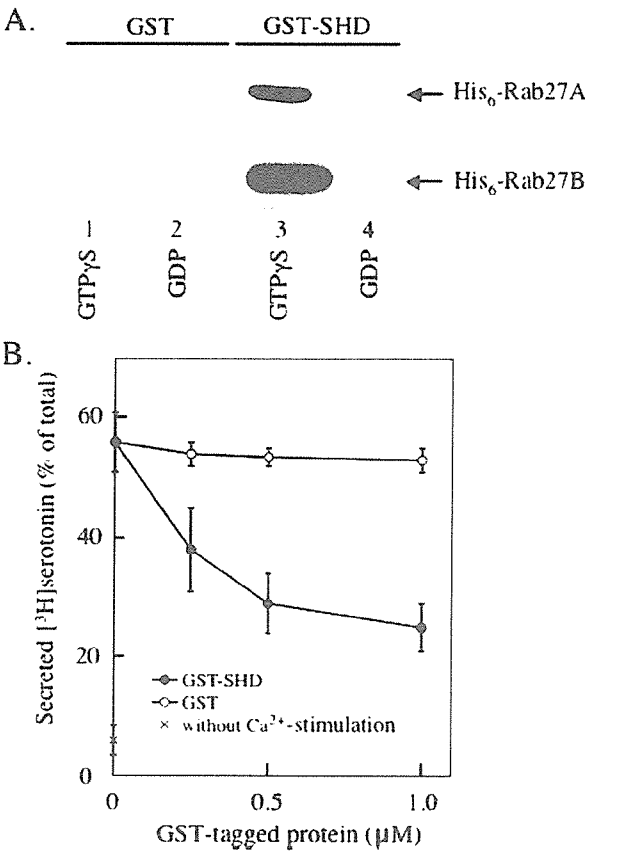

FIGURE 1. **Specific binding of SHD with GTP-Rab27 and its inhibitory effect on dense granule secretion in permeabilized platelets.** *A*, purified His_6-Rab27A (*upper panel*) and -Rab27B (*lower panel*) preloaded with GTPγS (*lanes 1* and *3*) or GDP (*lanes 2* and *4*) were incubated with glutathione beads coated with GST (*lanes 1* and *2*) and GST-SHD (*lanes 3* and *4*) at 4 °C for 1 h. After washing the beads, the bead-associated His_6-Rab27A and -Rab27B were detected by immunoblotting with anti-His_6 antibody as described under "Experimental Procedures." The data shown are representative of three independent experiments with similar results. *B*, permeabilized platelets were first incubated with various concentrations of GST (*open circles*) and GST-SHD (*closed circles*) at 4 °C for 30 min, and the Ca^{2+}-induced dense granule secretion ([^{3}H]serotonin) was analyzed as described under "Experimental Procedures." The secretion without the Ca^{2+} stimulation was shown (×). The results shown are expressed as means ± S.E. of three independent experiments.

of which are expressed in platelets (37). We incubated GTPγS (a non-hydrolyzable GTP analogue)-loaded and GDP-loaded His_6-Rab27 with GST-SHD-coated glutathione beads, and bead-associated Rab27 was analyzed by immunoblotting with anti-His_6 antibody. As shown in Fig. 1*A*, GST-SHD efficiently bound GTPγS-loaded Rab27A and Rab27B, with minimal binding to GDP-Rab27A and -Rab27B (Fig. 1*A*), indicating that the SHD specifically interacted with both GTP-Rab27A and GTP-Rab27B.

Next, we analyzed the involvement of Rab27 in the secretion using the SHD, which would sequester GTP-bound Rab27. In the assay, more than 50% of [^{3}H]serotonin preloaded into dense granules in permeabilized platelets was secreted within 1 min in response to Ca^{2+} stimulus at 30 °C, whereas the background secretion was 5–10% (Fig. 1*B*). The addition of GST-SHD, but not GST, in the assay efficiently inhibited the secretion in a concentration-dependent manner (Fig. 1*B*), supporting our

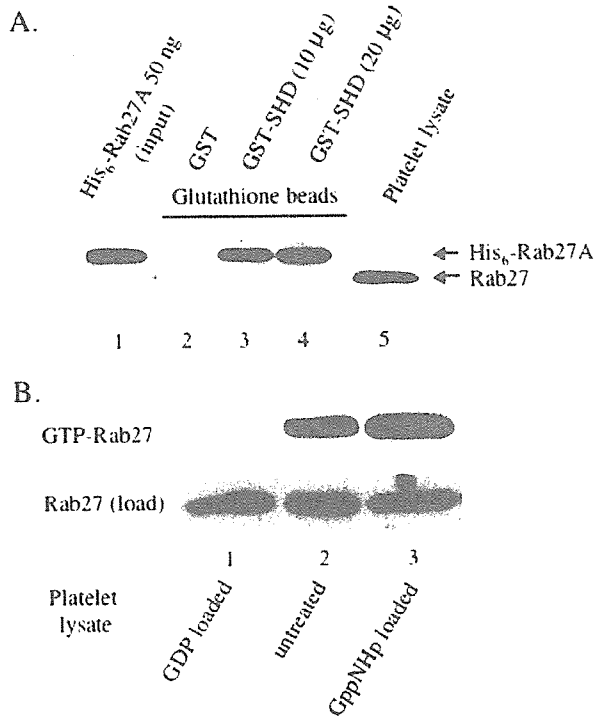

FIGURE 2. **A GTP-Rab27 pull-down assay using SHD revealed that GTP-Rab27 was predominant in unstimulated platelets.** *A*, GTP-loaded-His_6-Rab27A purified from *E. coli* (50 ng) (*lane 1*) was incubated at 4 °C for 30 min with glutathione beads coated with GST (*lane 2*), 10 μg of GST-SHD (*lane 3*), and 20 μg of GST-SHD (*lane 4*) followed by washing, and the bead-associated His_6-Rab27A was detected by immunoblotting with anti-Rab27 antibody as described under "Experimental Procedures." Platelet lysate isolated from 1 ml of blood was also analyzed (*lane 5*). The data shown are representative of three independent experiments with similar results. *B*, GTP-Rab27 in platelet lysate isolated from 1 ml of whole blood (*lane 2*) was incubated with glutathione beads coated with 10 μg of GST-SHD at 4 °C for 30 min, and bead-associated Rab27 was detected by immunoblotting with anti-Rab27 antibody as described under "Experimental Procedures." As controls, the same amounts of platelet lysates loaded *in vitro* with GDP (*lane 1*) or GppNHp (*lane 3*) were also analyzed in the same method. The data shown are representative of five independent experiments with similar results.

previous observation that Rab27 regulates dense granule secretion in platelets (28).

Establishment of GTP-Rab27 Pull-down Assay with SHD of Slac2-b—Most of Rab27 was present in the membrane fraction in platelets (34). To solubilize Rab27 from the membrane fraction in platelets, we used 0.5% Triton X-100, under which condition the interaction of the SHD with GTP-Rab27 was not affected. As shown in Fig. 2*A*, platelets ($\sim 5 \times 10^7$) isolated from 1 ml of blood contained ~50 ng of Rab27, determined using purified recombinant His_6-Rab27A as a reference. When the same amount (50 ng) of the recombinant His_6-Rab27A protein was used for a pull-down assay, almost all of the GTP-loaded form was bound to beads coated with 10 or 20 μg of GST-SHD but not to GST beads (Fig. 2*A*). Thus, this GST-SHD pull-down assay was established, and we used this method to evaluate the GTP-Rab27 levels in platelets.

Evaluation of GTP-Rab27 Level in Platelets—Using this pull-down assay, we evaluated the ratio of GTP-bound form of Rab27 in platelets. The results were calibrated as described previously (13), where the GDP/GTP-bound status of Rab3D in pancreatic acini was evaluated by their pull-down assay using a Rab3-effector RIM-1 (13). They solubilized pancreatic acinar cells, and the cell lysates were loaded with GTPγS or GDP. The amount of GST-RIM-1-associated Rab3D loaded with GTPγS was defined as 100%, and that loaded with GDP was defined as 0% (13). Here, we analyzed the GDP/GTP status of Rab27 in platelets and found that more than 70% (74.3 ± 3.0%, means ± S.E. of five individuals) of Rab27 was the GTP-bound form in unstimulated platelets (Fig. 2*B*).

We also evaluated the GDP/GTP-bound status of Rab27 by the thin layer chromatography method. Isolated platelets were first incubated at 37 °C for 3 h with [^{32}P]phosphorus that would be incorporated into GTP and GDP in platelets. As shown below (see Fig. 4*B*), nucleotide bound to immunoprecipitated Rab27 was predominantly GTP (62.7 ± 4.7%, means ± S.E. of three individuals). Thus, we obtained consistent results both by the pull-down and by the thin layer chromatography methods. We concluded that Rab27 was predominantly in the GTP-bound form in unstimulated platelets.

High Level of GTP-bound Rab27 Was Maintained by Constitutive GDP/GTP Exchange Activity in Platelets—We analyzed how the high level of GTP-Rab27 was maintained in unstimulated platelets. To examine this issue, permeabilized platelets were incubated in Buffer A (calculated free Ca^{2+} concentration was ~20 nM) (36) without the addition of ATP or platelet cytosol, where GTP would also be depleted by diffusion. In the platelets, the GTP-Rab27 level drastically decreased in a time-dependent manner measured by the Rab27 pull-down assay (Fig. 3, *A* and *C*), indicating that Rab27 in platelets was not fixed to be in the GTP-bound form. On the other hand, the same treatment of permeabilized platelets at 4 °C did not decrease GTP-Rab27 (Fig. 3*A*), indicating that this reaction is temperature-dependent. Importantly, this decrease was rescued by the addition of GTP in the system (Fig. 3, *B* and *C*), indicating that the high level of GTP-bound Rab27 was maintained most likely by GDP/GTP exchange reaction.

We examined whether the GDP/GTP exchange reaction indeed occurred in unstimulated platelets. We incubated permeabilized platelets with 10 μM [α-^{32}P]GTP at 30 °C in the absence of platelet cytosol. As shown in Fig. 3*D*, GTP-Rab27-associated radioactivity increased in a time-dependent manner, whereas amounts of GTP-Rab27 pulled down by the SHD were constant at any time point (data not shown), indicating that GDP/GTP exchange continuously took place to maintain the high level of GTP-Rab27 in unstimulated platelets. The rate of [α-^{32}P]GTP binding to endogenous Rab27 in permeabilized platelets was 0.032/min. Recombinant Rab27A protein purified from *E. coli in vitro* was examined in the same condition. The rate of [α-^{32}P]GTP binding to recombinant Rab27A was 0.0035/min (data not shown). Therefore, the GDP/GTP exchange rate for Rab27 in platelets was ~9 times faster than that of recombinant Rab27A. Since the exchange was so efficient in permeabilized platelets, in which the cytosol was extensively depleted due to diffusion, it is likely that the Rab27 GDP/GTP exchange factor, if any, is primarily membrane-associated.

GTP-bound Rab27 Decreased upon Granule Secretion through Enhanced GTP Hydrolysis Activity—We next examined the effect of granule secretion induced by an agonist on the

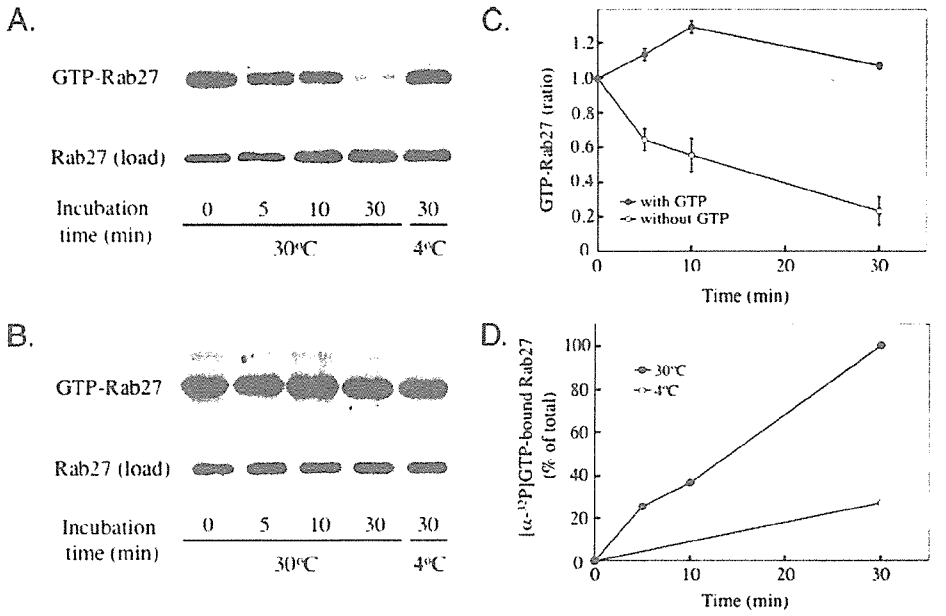

FIGURE 3. **Time-dependent decrease of GTP-Rab27 in permeabilized platelets, which was rescued by addition of GTP.** *A and B*, permeabilized platelets were incubated without the exogenous addition of ATP or platelet cytosol for the indicated periods at 30 °C or 4 °C, in the absence (*A*) or presence (*B*) of 1 mM GTP. GTP-Rab27 (*upper panels*) was measured by the GTP-Rab27 pull-down assay as described under "Experimental Procedures." The total Rab27 in the samples was shown in the *lower panels*. The data shown are representative of three independent experiments with similar results. *C*, time-dependent relative changes of GTP-Rab27 shown in *A* and *B* were presented using the GTP-Rab27 ratio at time 0 as a standard (1.0). The results shown are expressed as means ± S.E. of three independent experiments. *D*, permeabilized platelets were incubated with [α-^{32}P]GTP at 10 μM (10,000 cpm/pmol) for the indicated periods at 30 °C or 4 °C, and then GTP-Rab27 was pulled down by GST-SHD beads followed by quantification of [α-^{32}P]GTP as described under "Experimental Procedures." The results shown are representative of two independent experiments with similar results.

GDP/GTP status of Rab27. Upon 0.5 units/ml thrombin stimulation at 30 °C, GTP-Rab27 decreased from 74.3 ± 3.0 to 27.1 ± 6.3% at 3 min in intact platelets quantified by the pull-down assay (Fig. 4*A*). Similar results were obtained by the thin layer chromatography (Fig. 4*B*). After the thrombin stimulation for 3 min, GTP-Rab27 decreased from 62.7 ± 4.7 to 31.4 ± 1.4%, whereas GDP-Rab27 increased from 37.3 ± 4.7 to 68.6 ± 1.4%. Thus, Rab27-bound GTP drastically decreased with concomitant increase of Rab27-bound GDP upon stimulation, indicating that GTP hydrolysis of Rab27 was enhanced upon stimulation. The rate of GTP hydrolysis on Rab27 in thrombin-stimulated intact platelets in the thin layer chromatography method was 0.104/min. The rate of [γ-^{32}P]GTP hydrolysis on recombinant Rab27A purified from *E. coli* was 0.0056/min (data not shown). Therefore, the GTP hydrolysis velocity on Rab27 in stimulated platelets was ~18 times faster than that of recombinant Rab27A.

Decrease of GTP-Rab27 was also observed in permeabilized platelets undergoing the Ca^{2+}-induced granule secretion (Fig. 5*A*), and the degree of decrease was similar to that in thrombin-stimulated intact platelets (Fig. 4*A*). To examine whether GDP/GTP exchange activity was altered during the Ca^{2+}-induced granule secretion, permeabilized platelets were first incubated with [α-^{32}P]GTP, which would be loaded to small GTPases including Rab27 followed by the addition of excess non-labeled GTP. These platelets were incubated with ATP and platelet cytosol with or without Ca^{2+} stimulation. Then, time-dependent change of [α-^{32}P]GTP-Rab27 was compared. As shown in Fig. 5*B*, [α-^{32}P]GTP levels associated with immunoprecipitated Rab27 decreased over time similarly with or without Ca^{2+} stimulation. Since [α-^{32}P]GTP level associated with immunoprecipitated Rab27 would be affected by GDP/GTP exchange but not GTP hydrolysis, these results indicated that the GDP/GTP exchange activity was not affected upon stimulation.

Granule secretion is triggered by elevation of Ca^{2+} concentration (38). Since calcium ions regulate many cellular functions, we tried to address which triggered the decrease of GTP-Rab27, elevated Ca^{2+} concentration or secretion itself. We addressed this issue by using NEM, which is an inhibitor of an essential regulator of the SNARE system, NEM-sensitive factor. NEM inhibited the Ca^{2+}-induced dense granule secretion in a concentration-dependent manner in permeabilized platelets (Fig. 6*A*) as shown previously (39). Under these conditions, NEM treatment inhibited the decrease of the GTP-Rab27 level, although permeabilized platelets were stimulated with high concentration of Ca^{2+} (Fig. 6*B*). These data indicated that the fusion of the granules with plasma membrane, rather than the elevation of Ca^{2+} concentration, is required for enhancement of Rab27-associated GTP hydrolysis.

GTP Hydrolysis of Rab27 Did Not Appear Essential for the Dense Granule Secretion—To find out the implication of the high level of GTP-bound Rab27 and its secretion-dependent GTP hydrolysis, we tried to address whether GTP hydrolysis was required for granule secretion. It is well known that non-hydrolyzable GTP analogue at 100 μM promotes the Ca^{2+}-independent granule secretion in permeabilized platelets (40). However, in permeabilized platelets preincubated with a lower concentration of GppNHp at 10 μM, we observed a significant increase of the granule secretion upon Ca^{2+} stimulation (in Fig. 7*A*, compare *lane 4* and *lane 5*)($p < 0.01$), although the secretion level without Ca^{2+} stimulation was rather high (Fig. 7*A*, *lane 4*). Importantly, the Ca^{2+}-dependent secretion was reduced by the addition of the SHD (Fig. 7*A*, compare *lane 5* and *lane 6*)($p < 0.05$), indicating that Rab27 was involved in this secretion. Under this condition, in contrast to GTP-bound Rab27 (Fig. 7*B*, *lanes 1–3*), the GppNHp-bound form of Rab27 did not decrease upon granule secretion measured by the pull-down assay, indicating that the majority of Rab27 remained bound to GppNHp in the permeabilized platelets (Fig. 7*B*, *lanes 4–6*). Taken together, GTP hydrolysis of Rab27 did not appear necessary for the induction of granule secretion in platelets.

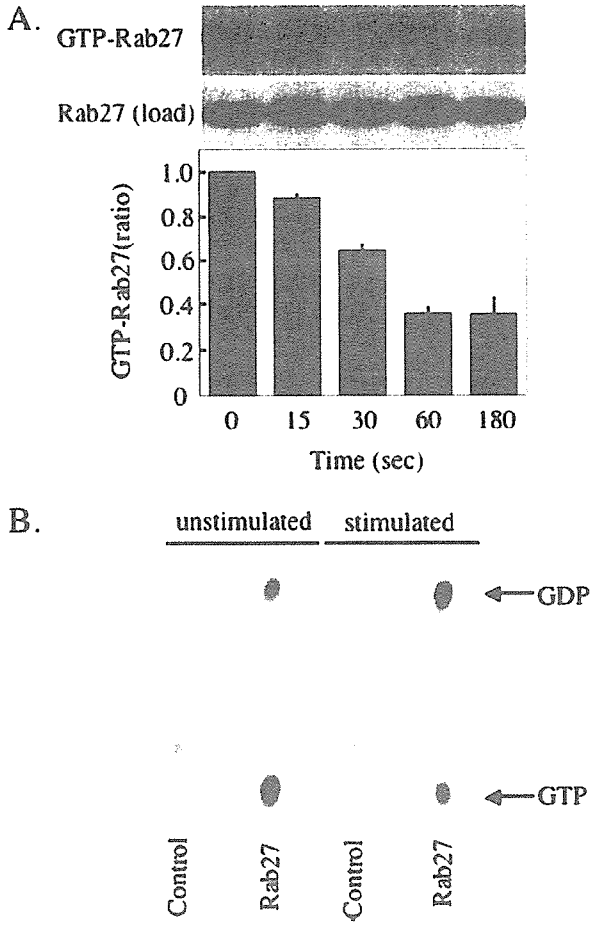

FIGURE 4. **GTP-Rab27 decreased upon granule secretion through enhanced GTP hydrolysis activity.** *A*, isolated platelets were stimulated with 0.5 units/ml thrombin for the indicated periods at 30 °C. Then, GTP-Rab27 (*upper panel*) was measured by the GTP-Rab27 pull-down assay as described under "Experimental Procedures." The total Rab27 in the samples was shown in the *lower panel*. Relative changes of GTP-Rab27 were presented using the GTP-Rab27 ratio at time 0 as a standard (1.0). The data shown are expressed as means ± S.E. of three independent experiments. *B*, isolated platelets were labeled with [^{32}P]phosphorus and then stimulated with 0.5 units/ml thrombin at 30 °C for 3 min. Rab27 was immunoprecipitated, and the bound nucleotides were analyzed by thin layer chromatography as described under "Experimental Procedures." The results shown are representative of three independent experiments with similar results.

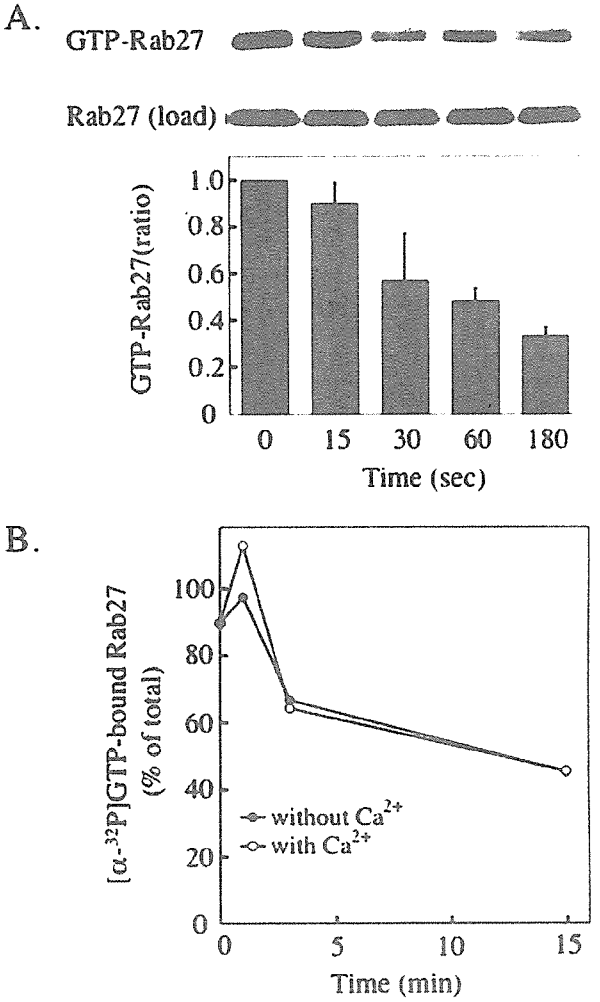

FIGURE 5. **The decrease of the GTP-Rab27 ratios upon the Ca^{2+}-induced secretion was not dependent on alteration of GDP/GTP exchange activity.** *A*, permeabilized platelets were stimulated in the presence of platelet cytosol and ATP by 20 μM Ca^{2+} for the indicated periods at 30 °C, and GTP-Rab27 (*upper panel*) was measured by the GTP-Rab27 pull-down assay as described under "Experimental Procedures." The total Rab27 in the samples was shown in the *lower panel*. Relative changes of GTP-Rab27 were presented using the GTP-Rab27 ratio at time 0 as a standard (1.0). The data shown are expressed as means ± S.E. of three independent experiments. *B*, permeabilized platelets were incubated with 10 μM [α-^{32}P]GTP at 30 °C for 30 min followed by the addition of cold excess GTP at 1 mM. These platelets were then incubated with or without 20 μM Ca^{2+} at 30 °C for the indicated periods, and the radioactivity associated with immunoprecipitated Rab27 was measured as described under "Experimental Procedures." The results shown are representative of two independent experiments with similar results.

DISCUSSION

In this study, we have analyzed the GDP/GTP cycle of endogenous Rab27 in platelets during regulated exocytosis and demonstrated that Rab27 was predominantly present in the GTP-bound form in unstimulated platelets and GTP-bound Rab27 decreased upon granule secretion. The activation status of Rab27 was regulated by constitutive GDP/GTP exchange activity and secretion-dependent GTP hydrolysis activity. Furthermore, we showed that GTP hydrolysis of Rab27 would not be essential for inducing the secretion. With these experimental results, we propose that the function of Rab27 in the platelet secretion is to maintain the granules in a preparative status for the secretion rather than to mediate the secretion signal.

We have established two methods for quantifying GTP-Rab27. One is the pull-down method in which we use the GTP-Rab27-binding domain, SHD, of a Rab27-specific effector molecule, Slac2-b (29). Since this SHD specifically interacted with GTP-Rab27 (Fig. 1*A*) and the interaction was unaffected by the detergent to solubilize Rab27, we could obtain reproducible results by this method. Another method is the thin layer chromatography method in which radioactive nucleotide bound to immunoprecipitated Rab27 was analyzed. The results obtained by these two independent methods were coincided. In contrast to the thin layer chromatography, which utilizes high levels of radioactivity and much primary antibodies, the pull-down assay is a preferred method to obtain equivalent results. Therefore, most of the experiments were performed with the pull-down assay, and key experiments for critical confirmation were performed with both methods.

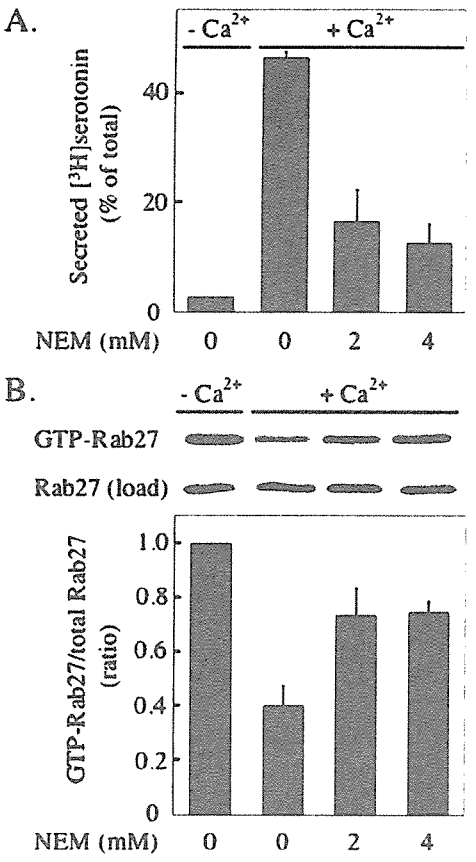

FIGURE 6. **The Ca^{2+} stimulation did not induce the decrease of GTP-Rab27 ratios when the secretion was inhibited by NEM in permeabilized platelets.** *A*, permeabilized platelets were incubated in the presence of platelet cytosol and ATP with various concentration of NEM at 4 °C for 30 min followed by the Ca^{2+} stimulation at 30 °C for 1 min. The Ca^{2+}-induced dense granule secretion was analyzed as described under "Experimental Procedures." The data shown are expressed as means ± S.E. of three independent experiments. *B*, GTP-Rab27 (*upper panel*) in these platelets was measured by the GTP-Rab27 pull-down assay as described under "Experimental Procedures." The total Rab27 in the samples was shown in the *lower panel*. Relative changes of GTP-Rab27 were presented using the GTP-Rab27 ratio at time 0 as a standard (1.0). The data shown are expressed as means ± S.E. of three independent experiments.

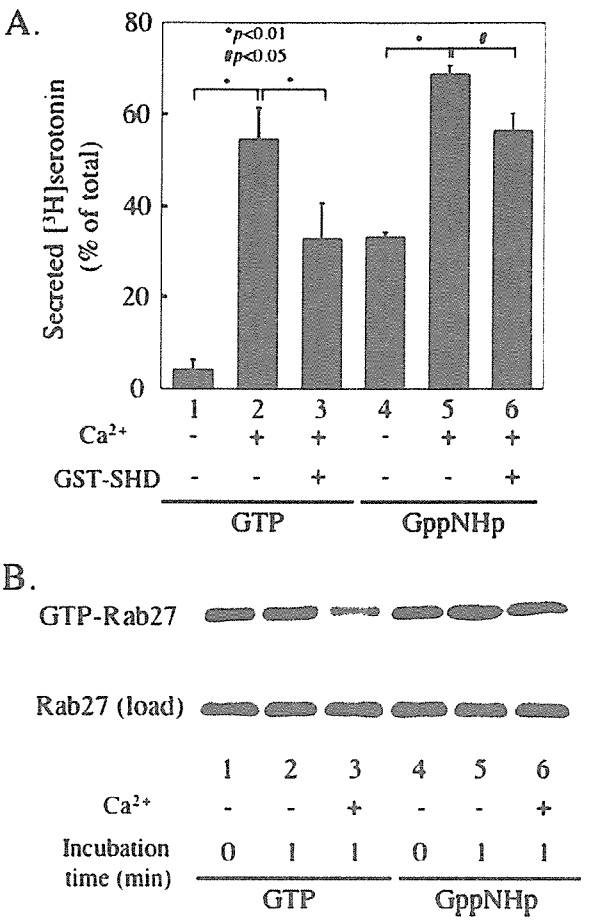

FIGURE 7. **GTP hydrolysis of Rab27 did not appear essential for the dense granule secretion.** *A*, permeabilized platelets were incubated with 10 μM GTP (*lanes 1–3*) or GppNHp (*lanes 4–6*) in the absence of platelet cytosol and ATP at 30 °C for 15 min followed by the addition of platelet cytosol and ATP. These permeabilized platelets were incubated with (*lanes 3* and *6*) or without (*lanes 1, 2, 4,* and *5*) 1 μM GST-SHD at 4 °C for 15 min. These permeabilized platelets were incubated with or without Ca^{2+} for 1 min, and secreted [^{3}H]serotonin was analyzed as described under "Experimental Procedures." The results shown are expressed as means ± S.E. of five independent experiments. *, $p < 0.01$, *lane 1 versus lane 2*, *lane 2 versus lane 3*, and *lane 4 versus lane 5*. #, $p < 0.05$, *lane 5 versus lane 6*. *B*, GTP- (or GppNHp-) Rab27 (*upper panel*) in these platelets was measured by the GTP-Rab27 pull-down assay as described under "Experimental Procedures." The total Rab27 in the samples was shown in the *lower panel*. The results shown are representative of three independent experiments with similar results.

We investigated the mechanism by which GTP-Rab27 is maintained at such a high level. Two possibilities were conceivable; GTP bound to Rab27 is statically kept without entering the GDP/GTP cycle, or the GTP-bound form is maintained in a dynamic equilibrium between GTP hydrolysis and GDP/GTP exchange activities. Here, the data demonstrated the high rates of nucleotide exchange for Rab27 in unstimulated platelets. First, GTP-Rab27 levels decreased in permeabilized platelets without the addition of GTP in the milieu. Second, this decrease was rescued by the addition of GTP in the system. Third, [α-^{32}P]GTP added in the system was incorporated to Rab27 in a time-dependent manner, whereas total GTP-Rab27 levels were not changed. Thus, the high level of GTP-bound Rab27 in unstimulated platelets was maintained by constitutive GDP/GTP exchange activity. Since we detected GDP/GTP exchange activity for Rab27 in permeabilized platelets, where the cytosol was extensively depleted, the majority of the GDP/GTP exchange activity could be membrane-associated.

Rybin *et al.* (41) have examined the GDP/GTP cycle of Rab5 on purified early endosomal membrane in the steady states by experiments analyzing xanthosine 5′-triphosphate bound to mutant Rab5, which preferentially binds xanthosine 5′-triphosphate instead of GTP. They demonstrated that Rab5 activity is regulated in a dynamic equilibrium by constitutive GTP hydrolysis activity on purified early endosome membrane. Then, they speculated that Rab5 undergoes multiple cycles of nucleotide binding and hydrolysis on the early endosome membrane (41).

Since GDP-bound Rab GTPases could be present in cytosol by forming a complex with RabGDI, the data that most of Rab27 localizes in the membrane fraction (33) could reflect the predominant existence of Rab27 in the GTP-bound form in platelets. Since GDP/GTP exchange occurred in Rab27 in permeabilized platelets without the addition of platelet cytosol containing RabGDI (Fig. 3, *A*, *B*, and *D*), Rab27 appears to undergo multiple GDP/GTP cycle on the membrane, similar to Rab5, without recycling between cytosol and membrane.

Here, we demonstrated that the high level of GTP-Rab27 markedly decreased upon stimulation in platelets due to enhanced Rab27 GTP hydrolysis activity. Since the GDP/GTP exchange activity for Rab27 appeared unchanged by granule secretion (Fig. 5*B*), this decrease of GTP-Rab27 would be exclusively due to the enhanced GTP hydrolysis activity upon stimulation. The granule secretion is triggered by increased Ca^{2+} concentration. However, the Rab27 GTP hydrolysis activity was not enhanced by increased Ca^{2+} concentration alone. It was coupled with granule secretion *per se* since increased Ca^{2+} concentration did not decrease the GTP-Rab27 level when the secretion was inhibited by NEM.

What is the implication of the high active status of Rab27 in unstimulated platelets and GTP hydrolysis upon granule secretion? If GTP hydrolysis of Rab27 is not required for the secretion, the predominant presence of Rab27 in its active form would imply that Rab27 does not mediate the secretion signal directly but rather plays a role to maintain the vesicles in the preparative state for secretion. If GTP hydrolysis of Rab27 is required for fusion, GTP-Rab27 would function as a negative regulator, where the secretion signal induces GTP hydrolysis of Rab27 to trigger the secretion. To date, two types of functional mechanisms of GTPases are known. Some require GTP hydrolysis for the function, and the others do not require it. For examples, elongation factor EF-Tu requires GTP hydrolysis to perform the proofreading of elongation of the correct amino acid at the end of peptide under production (42). On the other hand, the GTP-bound form of Rab5 is the active form, which induces membrane docking/fusion of early endosomes without requiring GTP hydrolysis (11, 41). Therefore, elucidation of the implication of GTP hydrolysis of Rab27 is essential to understand the functional mechanism of Rab27 in the regulation of the secretion.

To address this issue, we used non-hydrolyzable GTP analogue, GppNHp, in the assay system with permeabilized platelets. It is well known that non-hydrolyzable GTP analogue at 100 μM promotes the Ca^{2+}-independent granule secretion in permeabilized platelets (40). However, in permeabilized platelets preincubated with a lower concentration of GppNHp at 10 μM, we observed a significant increase of the granule secretion upon Ca^{2+} stimulation. In this experiment, the GTP-Rab27 level did not decrease by the granule secretion, suggesting that almost all Rab27 bound GppNHp. Furthermore, the Ca^{2+}-induced secretion in the presence of 10 μM GppNHp was inhibited by the addition of the GTP-Rab27-binding domain, SHD (Fig. 7*A*, *lane 6*), indicating that Rab27 played a role for inducing the secretion. Therefore, we would conclude that GTP-Rab27 is the active form and GTP hydrolysis of Rab27 does not appear necessary for dense granule secretion in platelets.

Since Rab27 in platelets is predominantly present in its GTP-bound form and GTP hydrolysis appears unnecessary for the secretion, it is likely that GTP-Rab27 would not mediate extracellular signals but rather keep the vesicles in a preparative state for the secretion. Since increased Ca^{2+} concentration is the trigger of the secretion (38), the calcium ion signal would be mediated by a calcium-binding protein such as a Rab27 effector molecule Munc13-4 containing Ca^{2+}-binding C2 domains (28), and protein kinase C (33).

Nevertheless, we cannot completely exclude the possibility that GTP hydrolysis of Rab27 is required for the granule secretion due to some limitations in the experiments shown in Fig. 7 to address the requirement of GTP hydrolysis of Rab27 for the secretion. First, other GTPases as well as Rab27 would bind GppNHp in permeabilized platelets. Some of these GTPases might bypass the need for GTP hydrolysis of Rab27. Second, the spans of the Ca^{2+}-induced secretion and the inhibition by the SHD were relatively small in the assay due to rather high levels of secretion without Ca^{2+} stimulation in the presence of GppNHp. Although the differences are statistically significant, additional experiments would be required for the definite conclusion.

At this time, the biological implication of the secretion-dependent GTP hydrolysis of Rab27 remains unclear. It might play a role in recycling of Rab27 from the plasma membrane after one cycle of the secretion is completed.

Platelets contain many small GTPases, such as Ras, RhoA, Rap1, and Ral, that are predominantly present in their GDP-bound forms and transiently become GTP-bound forms upon stimulation in platelets (43–46). In contrast to these small GTPases, the GDP/GTP cycle of Rab27 appears unique. Given that Rab27 in platelets was predominantly in the GTP-bound form, the GDP/GTP exchange activity would be more dominant than the GTP hydrolysis activity in unstimulated platelets. Furthermore, this GDP/GTP exchange activity for Rab27 was not changed by the elevation of Ca^{2+} concentration (Fig. 5*B*), unlike that for other small GTPases (12, 46). Very recently, the GDP/GTP cycle of Arf6 has been demonstrated to be similar to that of Rab27 (46), where most of Arf6 is present in its GTP-bound form and GTP-Arf6 is decreased by agonist stimulation to regulate Rho family GTPases in platelets, although it has not been addressed whether GTP hydrolysis plays a role or not in its functions (46).

In pancreatic acini, most of Rab3D has been demonstrated to be in the GTP-bound form (13), although the GDP/GTP status of Rab3D in response to cellular stimulus has not been addressed. Since the Rab3 family is implicated in regulated exocytosis and related to Rab27 in the primary structure (16), the predominant GTP-bound form in the resting cells might be common in Rab GTPases implicated in regulated exocytosis.

Here, we showed that Rab27 in unstimulated platelets was predominantly present in the GTP-bound active form, which was regulated by its constitutive GDP/GTP exchange activity in a dynamic equilibrium and that this high level of GTP-Rab27 drastically decreased upon granule secretion due to enhanced GTP hydrolysis activity. To elucidate the molecular mechanism of the regulation in the secretion, it would be crucial to identify GTPase-activating protein and GDP/GTP exchange factor for Rab27 in platelets and characterize their functions in the platelet secretion.

Acknowledgments—We are grateful to Dr. Yoshinori Nozawa for providing a plasmid containing Rab27A and to Kazusa DNA Research Institute for providing KIAA0624. We are also grateful to the Kyoto Red Cross Blood Center for providing platelet pellets. We thank Dr. Heidi McBride (Ottawa) and Dr. Yasuyuki Fujita (London) for critical reading of the manuscript and Tomoko Matsubara for excellent technical assistance.

REFERENCES

1. Chen, Y. A., and Scheller, R. H. (2001) *Nat. Rev. Mol. Cell. Biol.* **2,** 98–106
2. Zerial, M., and McBride, H. (2001) *Nat. Rev. Mol. Cell. Biol.* **2,** 107–117
3. Takai, Y., Sasaki, T., and Matozaki, T. (2001) *Physiol. Rev.* **81,** 153–208
4. Jordens, I., Marsman, M., Kuijl, C., and Neefjes, J. (2005) *Traffic* **6,** 1070–1077
5. Ullrich, O., Horiuchi, H., Bucci, C., and Zerial, M. (1994) *Nature* **368,** 157–160
6. Soldati, T., Shapiro, A. D., Svejstrup, A. B., and Pfeffer, S. R. (1994) *Nature* **369,** 76–78
7. Horiuchi, H., Giner, A., Hoflack, B., and Zerial, M. (1995) *J. Biol. Chem.* **270,** 11257–11262
8. Dirac-Svejstrup, A. B., Sumizawa, T., and Pfeffer, S. R. (1997) *EMBO J.* **16,** 465–472
9. Satoh, T., Endo, M., Nakafuku, M., Akiyama, T., Yamamoto, T., and Kaziro, Y. (1990) *Proc. Natl. Acad. Sci. U. S. A.* **87,** 7926–7929
10. Bucci, C., Parton, R. G., Mather, I. H., Stunnenberg, H., Simons, K., Hoflack, B., and Zerial, M. (1992) *Cell* **70,** 715–728
11. Stenmark, H., Parton, R. G., Steele-Mortimer, O., Lutcke, A., Gruenberg, J., and Zerial, M. (1994) *EMBO J.* **13,** 1287–1296
12. Barbieri, M. A., Roberts, R. L., Gumusboga, A., Highfield, H., Alvarez-Dominguez, C., Wells, A., and Stahl, P. D. (2000) *J. Cell Biol.* **151,** 539–550
13. Chen, X., Ernst, S. A., and Williams, J. A. (2003) *J. Biol. Chem.* **278,** 50053–50060
14. Nagata, K., Satoh, T., Itoh, H., Kozasa, T., Okano, Y., Doi, T., Kaziro, Y., and Nozawa, Y. (1990) *FEBS Lett.* **275,** 29–32
15. Chen, D., Guo, J., Miki, T., Tachibana, M., and Gahl, W. A. (1997) *Biochem. Mol. Med.* **60,** 27–37
16. Fukuda, M. (2005) *J. Biochem. (Tokyo)* **137,** 9–16
17. Stinchcombe, J. C., Barral, D. C., Mules, E. H., Booth, S., Hume, A. N., Machesky, L. M., Seabra, M. C., and Griffiths, G. M. (2001) *J. Cell Biol.* **152,** 825–834
18. Haddad, E. K., Wu, X., Hammer, J. A., III, and Henkart, P. A. (2001) *J. Cell Biol.* **152,** 835–842
19. Yi, Z., Yokota, H., Torii, S., Aoki, T., Hosaka, M., Zhao, S., Takata, K., Takeuchi, T., and Izumi, T. (2002) *Mol. Cell. Biol.* **22,** 1858–1867
20. Neeft, M., Wieffer, M., de Jong, A. S., Negroiu, G., Metz, C. H., van Loon, A., Griffith, J., Krijgsveld, J., Wulffraat, N., Koch, H., Heck, A. J., Brose, N., Kleijmeer, M., and van der Sluijs, P. (2005) *Mol. Biol. Cell* **16,** 731–741
21. Goishi, K., Mizuno, K., Nakanishi, H., and Sasaki, T. (2004) *Biochem. Biophys. Res. Commun.* **324,** 294–301
22. Wu, X. S., Rao, K., Zhang, H., Wang, F., Sellers, J. R., Matesic, L. E., Copeland, N. G., Jenkins, N. A., and Hammer, J. A., III (2002) *Nat. Cell Biol.* **4,** 271–278
23. Hume, A. N., Collinson, L. M., Rapak, A., Gomes, A. Q., Hopkins, C. R., and Seabra, M. C. (2001) *J. Cell Biol.* **152,** 795–808
24. Fukuda, M., Kuroda, T. S., and Mikoshiba, K. (2002) *J. Biol. Chem.* **277,** 12432–12436
25. Nagashima, K., Torii, S., Yi, Z., Igarashi, M., Okamoto, K., Takeuchi, T., and Izumi, T. (2002) *FEBS Lett.* **517,** 233–238
26. Brass, L. F. (2005) in *Hematology: The Molecular Basis of Platelet Activation* (Hoffman, R., Benz, E. J., Jr., Shattil, S. J., Furie, B., Cohen, H. J., Silberstein, L. E., and McGlave, P. eds) 4th Ed., pp. 1889–1914, Elsevier, NY
27. Horiuchi, H. (2006) *Ann. Med.* **38,** 162–172
28. Shirakawa, R., Higashi, T., Tabuchi, A., Yoshioka, A., Nishioka, H., Fukuda, M., Kita, T., and Horiuchi, H. (2004) *J. Biol. Chem.* **279,** 10730–10737
29. Kuroda, T. S., Fukuda, M., Ariga, H., and Mikoshiba, K. (2002) *J. Biol. Chem.* **277,** 9212–9218
30. Imai, A., Yoshie, S., Nashida, T., Shimomura, H., and Fukuda, M. (2004) *J. Cell Sci.* **117,** 1945–1953
31. Bhakdi, S., Weller, U., Walev, I., Martin, E., Jonas, D., and Palmer, M. (1993) *Med. Microbiol. Immunol. (Berl.)* **182,** 167–175
32. Yoshioka, A., Horiuchi, H., Shirakawa, R., Nishioka, H., Tabuchi, A., Higashi, T., Yamamoto, A., and Kita, T. (2001) *Ann. N. Y. Acad. Sci.* **947,** 403–406
33. Yoshioka, A., Shirakawa, R., Nishioka, H., Tabuchi, A., Higashi, T., Ozaki, H., Yamamoto, A., Kita, T., and Horiuchi, H. (2001) *J. Biol. Chem.* **276,** 39379–39385
34. Shirakawa, R., Yoshioka, A., Horiuchi, H., Nishioka, H., Tabuchi, A., and Kita, T. (2000) *J. Biol. Chem.* **275,** 33844–33849
35. Shirakawa, R., Higashi, T., Kondo, H., Yoshioka, A., Kita, T., and Horiuchi, H. (2005) *Methods Enzymol.* **403,** 778–788
36. Fabiato, A., and Fabiato, F. (1979) *J. Physiol. (Paris)* **75,** 463–505
37. Barral, D. C., Ramalho, J. S., Anders, R., Hume, A. N., Knapton, H. J., Tolmachova, T., Collinson, L. M., Goulding, D., Authi, K. S., and Seabra, M. C. (2002) *J. Clin. Investig.* **110,** 247–257
38. Knight, D. E., Hallam, T. J., and Scrutton, M. C. (1982) *Nature* **296,** 256–257
39. Polgar, J., and Reed, G. L. (1999) *Blood* **94,** 1313–1318
40. Coorssen, J. R., and Haslam, R. J. (1993) *FEBS Lett.* **316,** 170–174
41. Rybin, V., Ullrich, O., Rubino, M., Alexandrov, K., Simon, I., Seabra, M. C., Goody, R., and Zerial, M. (1996) *Nature* **383,** 266–269
42. Bourne, H. R. (1988) *Cell* **53,** 669–671
43. Franke, B., Akkerman, J. W., and Bos, J. L. (1997) *EMBO J.* **16,** 252–259
44. Bodie, S. L., Ford, I., Greaves, M., and Nixon, G. F. (2001) *Biochem. Biophys. Res. Commun.* **287,** 71–76
45. Wolthuis, R. M., Franke, B., van Triest, M., Bauer, B., Cool, R. H., Camonis, J. H., Akkerman, J. W., and Bos, J. L. (1998) *Mol. Cell. Biol.* **18,** 2486–2491
46. Choi, W., Karim, Z. A., and Whiteheart, S. W. (2006) *Blood* **107,** 3145–3152

Geriatr Gerontol Int 2006; 6: 205–208

Elucidation of the molecular mechanism of platelet activation: Dense granule secretion is regulated by small guanosine triphosphate-binding protein Rab27 and its effector Munc13-4

Hisanori Horiuchi, Ryutaro Shirakawa, Hirokazu Kondo, Tomohito Higashi, Mitsunori Kawato and Toru Kita

Department of Cardiovascular Medicine, Graduate School of Medicine, Kyoto University, Kyoto, Japan

Cardiovascular diseases such as myocardial and cerebral infarction are common critical diseases occurring more frequently in the elderly. The trigger of the diseases is platelet activation following plaque rupture or erosion. Investigation of the molecular mechanism in platelet activation has been exclusively performed pharmacologically. We have succeeded in establishing the granule secretion and aggregation assays using permeabilized platelets. These systems enabled us to examine the molecular mechanism in platelet activation with molecular biological and biochemical methods. Using these assay systems, we have been investigating the molecular mechanism of platelet activation. With a support grant from the Novartis Foundation for Gerontological Research, we found several molecules involved in the regulation. In this report, I present the progress in the research of the granule secretion mechanism in activated platelets, which was reported in the Japanese Geriatric Society Meeting in 2005.

Keywords: dense granule, exocytosis, Munc13-4, platelet, Rab27.

Introduction

Cardiovascular diseases such as myocardial and cerebral infarction are common critical diseases occurring more frequently in the elderly. These are caused by arterial occlusion by thrombus where the trigger is platelet activation following plaque rupture or erosion. Activated platelets adhere to the injured vessel wall, release many active substances stored in α- and dense granules, aggregate to form white thrombus, and undergo shape change.[1] In spite of the critical roles, the molecular mechanisms underlying platelet activation remain unclear, mainly due to difficulty in using a molecular biological method in the investigation of platelets lacking nuclei.

We have succeeded in establishing assays to examine the mechanisms of dense granule secretion by measuring secreted [^{3}H]serotonin and the Ca^{2+}-induced aggregation using isolated platelets permeabilized with the bacterial toxin streptolysin-O (SLO). Supported by a grant from the Novartis Foundation for Gerontological Research, we have investigated the molecular mechanism of platelet activation using the semi-intact assay systems. We have directly demonstrated that protein kinase C-α (PKC-α) regulates platelet aggregation.[2] The aggregation is regulated by the adaptor protein ShcA through interaction with the tyrosine-phosphorylated

Accepted for publication 12 July 2006.

Correspondence: Dr Hisanori Horiuchi, Department of Cardiovascular Medicine, Graduate School of Medicine, Kyoto University, Kyoto 606-8507, Japan. Email: horiuchi@kuhp.kyoto-u.ac.jp

The report of this research was granted by the Novartis Foundation for Gerontological Research.

doi: 10.1111/j.1447-0594.2006.00344.x